

Summary

2	1	Introduction	3
3	2	Pixel detectors	4
4	2.1	Signal formation	4
5	2.2	CCDs	5
6	2.3	Hybrid pixels	5
7	2.4	CMOS MAPS and DMPAS	6
8	2.4.1	DMAPS: large and small fill factor	7
9	2.4.2	A modified sensor	7
10	2.5	Analog front end	8
11	2.5.1	Preamplifier	8
12	2.6	Readout logic	10
13	3	Use of pixel detectors	13
14	3.1	Tracking in HEP	13
15	3.1.1	Hybrid pixels at LHC: ATLAS, CMS and LHC-b	14
16	3.1.2	A DEPFET example: Belle-II	15
17	3.1.3	CMOS MAPS: ALICE and STAR	15
18	3.2	Application in imaging	15
19	3.2.1	Medipix	15
20	3.2.2	Applicability to FLASH radiotherapy	16
21	4	TJ-Monopix1	17
22	4.1	The sensor	18
23	4.2	Front end	20
24	4.2.1	ALPIDE-like	20
25	4.3	Readout logic	21
26	4.3.1	Dead time measurements	24
27	5	Arcadia-MD1	26
28	5.1	The sensor	26
29	5.2	Readout logic and data structure	26
30	5.2.1	Matrix division and data-packets	26
31	6	Threshold and noise characterization	30
32	6.1	Threshold and noise: figure of merit for pixel detectors	30
33	6.2	TJ-Monopix1 characterization	31
34	6.3	ARCADIA-MD1 characterization	31
35	7	Test beam measurements	32
36	A	Pixels detector: a brief overview	33
37	A.1	Radiation damages	33
38	B	FLASH radiotherapy	35
39	B.1	Cell survival curves	35
40	B.2	FLASH effect	36

⁴¹ **Bibliography**

37

⁴² Characterization of monolithic CMOS pixel sensors for charged particle detectors and for high
⁴³ intensity dosimetry

⁴⁴ **Chapter 1**

⁴⁵ **Introduction**

⁴⁶ Pixel detectors, members of the semiconductor detector family, have significantly been used since
⁴⁷ () at the first accelerator experiments for energy and position measurement. Because of their
⁴⁸ dimension (today $\sim 30 \mu\text{m}$ or even better) and their spatial resolution ($\sim 5\text{-}10 \mu\text{m}$), with the
⁴⁹ availability of technology in 1980s they proved to be perfectly suitable for vertex detector in the
⁵⁰ inner layer of the detector.

⁵¹ Technological development has been constant from then on and today almost every high energy
⁵² physics (HEP) experiment employs a pixels detector; hybrid pixel currently constitute the state-
⁵³ of-art for large scale pixel detector but experiments began to look at the more innovative monolithic
⁵⁴ active pixels (MAPS) as perspective for their future upgrades, as BelleII, or they already have
⁵⁵ installed them, as ALICE.

⁵⁶ Requirement imposed by accelerator are stringent and they will be even more with the increase
⁵⁷ of luminosity/intensity, in terms of radiation hardness, efficiency and occupancy, time resolution,
⁵⁸ material budget and power consumption.

⁵⁹ Qual è invece la richiesta per la dosimetria?

⁶⁰ While CCDs pioneered the use of silicon pixels for precision tracking,

62 Chapter 2

63 Pixel detectors

64 2.1 Signal formation

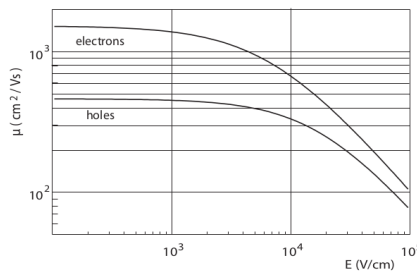
65 When a charge particle passes through a pixel and loses energy by ionization a part of that
 66 energy is used to generate electron-hole pairs (another part is used for other processes, as the
 67 lattice excitation) which are then separated by the electric field and collected at their respectively
 68 electrodes (p for holes and n for electrons)¹; by the drift of these charges, a signal i_e is generated
 69 on the electrode e as stated by the Shockley–Ramo's theorem:

$$i_e(t) = -q v(t) E_{WF,e} \quad (2.1)$$

70 where $v(t)$ is the instantaneous velocity of the charge q and E_{WF} is the weighting field, that is the
 71 field obtained biasing the electrode e with 1V and all the others with 0V. The drift velocity of the
 72 charge depends on the electric field and on the mobility of the particle:

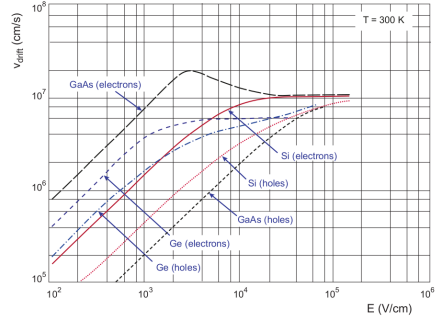
$$v = \mu(E) E \quad (2.2)$$

73 where $\mu(E)$ is a function of the electric field and is linear with E only for small E : at higher values
 74 the probability of interactions with optical phonons increases and the mobility drops and this leads
 75 to an independence of the velocity from the electric field (fig. 2.1b).



(a) Typical values for electrons and holes mobility in

silicon at room temperature are $\mu_n \sim 1450 \text{ cm}^2/\text{Vs}$, $\mu_h = 500$



(b) Drift velocity at room temperature in different semiconductors

76 The average energy needed to create a pair at 300 K in silicon is $w_i = 3.65 \text{ eV}$, that is more
 77 than the mean ionization energy because of the interactions with phonon, since for a minimum
 78 ionizing particle (MIP) the most probable value (MPV) of charge released in the semiconductor is
 79 0.28 keV/ μ , hence the number of e/h pairs is:

$$\langle \frac{dE}{dx} \rangle \frac{1}{w_i} \sim 80 \text{ e}/\text{h} \sim \frac{1.28 \cdot 10^{-2} fC}{\mu m} \quad (2.3)$$

¹Even if in principle both the electrode can be used to read a signal, for pixel detectors, where the number of channel and the complexity of readout are high, only one is actually used. In strip and pad detectors, instead, is more common a dual-side readout

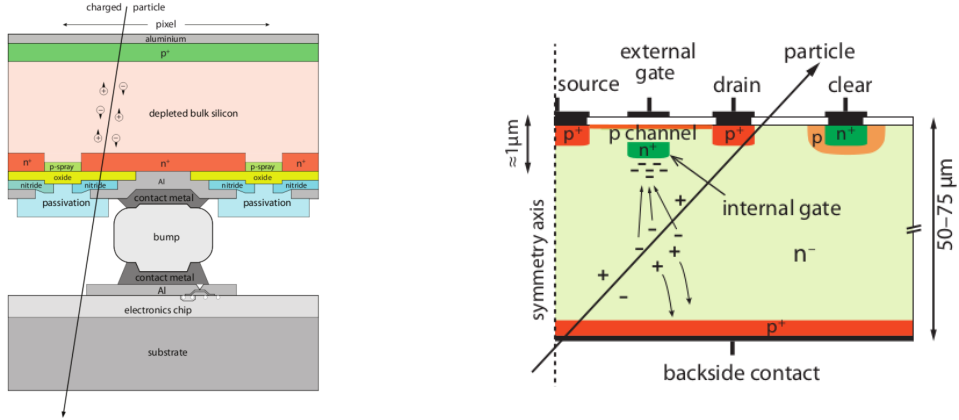


Figure 2.2: Concept cross-section of hybrid pixel (a) and of a DEPFET (b)

80 CON UN'INCERTEZZA CHE È RADICE DI N; ED EVENTUALEMTE SI AGGIUNGE IL
 81 FATTORE DI FANO NEL CASO DI ASSORBIMENTO TOTALE. IL FATTORE DI FANO È
 82 0.115 NELL SILICIO. ecc It is fundamental that pairs e/h are produced in the depleted region
 83 of the semiconductor where the probability of recombination with charge carriers is low to avoid
 84 loss of signals. Pixel detectors are then commonly reverse biased: a positive bias is given to the
 85 n electrode and a negative to the p to grow the depletion zone in the epitaxial layer below the
 86 electrode. The width of the depletion region is related with the external bias V_{ext} , the resistivity
 87 ρ and also with the dopant:

$$d_n \sim 0.55 \sqrt{\frac{\rho}{\Omega cm} \frac{V_{ext}}{V}} \mu m \quad (2.4) \quad d_p \sim 0.32 \sqrt{\frac{\rho}{\Omega cm} \frac{V_{ext}}{V}} \mu m \quad (2.5)$$

88

89

90 For that reason high resistivity wafers ($100 \Omega cm - k\Omega cm$) are typically preferred because they
 91 allow bigger depletion zone with smaller voltage bias.
 92

93 2.2 CCDs

94 ens of ms due to the need to transfer the charge signals pixel by pixel through a single output
 95 circuit For photon imaging the need of high assorbtion efficiency

96 2.3 Hybrid pixels

97 METTI IN EVIDENZAZ CHE PUOI FARE UN READOUT CON TECNOLOGIA CMOS Hybrid
 98 pixels are made of two parts (fig. 2.2a), the sensor and the electronics: for each pixel these two
 99 parts are welded together through microconnection (bump bond).
 100 They provide a practical system where readout and sensor can be optimized separately, although
 101 the testing is less easy-to-do since the sensor and the R/O must be connected together before.
 102 In addition, the particular and sophisticated procedure to bond sensor and ASIC (application spe-
 103 cific integrated circuit) makes them difficult to produce, delicate, especially when exposed to high
 104 levels of radiation, and also expensive.

105 A critical parameter for accelerator experiments is the material budget, which represents the main
 106 limit factor for momentum measurement resolution in a magnetic field; since hybrid pixels are
 107 thicker (\sim hundreds of μm) than monolithic ones (even less than $100 \mu m$), using the latter the
 108 material budget can be down by a third: typical value for hybrid pixels is $1.5 \% X_0$ per layer,
 109 while for monolithic $0.5 \% X_0$.

110 Among other disadvantages of hybrid pixels there is the bigger power consumption that implies,
 111 by the way, a bigger cooling system leading in turn to an increase in material too.

112

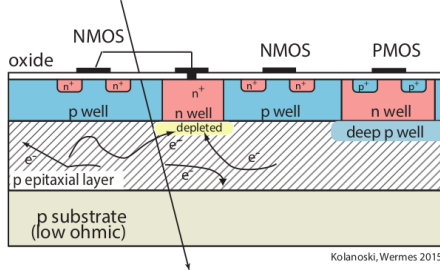


Figure 2.3: Concept cross-section of CMOS MPAS pixel

113 DEPFET are the first attempt towards the integration of the front end (FE) on the sensor bulk:
 114 they are typically mounted on a hybrid structure but they also integrate the first amplification
 115 stage.

116 Each pixel implements a MOSFET (metal-oxide-semiconductor field-effect transistor) transistor
 117 (a p-channel in fig. 2.2b): an hole current flows from source to drain which is controlled by the
 118 external gate and the internal gate together. The internal gate is made by a deep $n+$ implant
 119 towards which electrons drift after being created in the depletion region (to know how the signal
 120 is created in a pixel detector look at appendix A); the accumulation of electrons in the region
 121 underneath the n implant changes the gate potential and controls the transistor current.
 122 DEPFET typically have a good S/N ratio: this is principally due the amplification on-pixel and
 123 the large depletion region. But, since they need to be connected with ASIC the limiting factor still
 124 is the material budget.

125 2.4 CMOS MAPS and DMPAS

126 With respect to CCDs, the radiation tolerance could be greatly increased by sensing the signal
 127 charge within its own pixel, instead of transporting it over thousands of pixels. The readout
 128 speed could also be dramatically increased by in-pixel amplitude discrimination, followed by sparse
 129 readout of only the hit pixels Monolithic active pixels accommodate on the same wafer both the
 130 sensor and the front end electronics, with the second one implanted on top within a depth of about
 131 1 μm below the surface.

132 MAPS have been first proposed and realized in the 1990s and their usage has been enabled by the
 133 development of the electronic sector which guarantees the decrease in CMOS transistors dimension
 134 at least every two years, as stated by the Moore's law².

135 As a matter of fact the dimension of components, their organization on the pixel area and logic
 136 density are important issues for the design and for the layout; typically different decisions are taken
 137 for different purposes.

138 Monolithic active pixel can be distinguished between two main categories: MAPS and depleted
 139 MAPS (DMAPS).

140 MAPS (figure a 2.3) have typically an epitaxial layer in range 1-20 μm and because they are not
 141 depleted, the charge is mainly collected by diffusion rather than by drift. This makes the path of
 142 charges created in the bulk longer than usual, therefore they are slow (of order of 100 ns) and the
 143 collection could be partial especially after the irradiation of the detector (look at A for radiation
 144 damages), when the trapping probability become higher.

145 In figure 2.3 is shown as example of CMOS MAPS: the sensor in the scheme implements an
 146 n well as collection diode; to avoid the others n wells (which contain PMOS transistor) of the
 147 electronic circuit would compete in charge collection and to shield the CMOS circuit from the
 148 substrate, additionally underlying deep p well are needed. DMAPS are instead MAPS depleted
 149 with d typically in $\sim 25\text{-}150 \mu\text{m}$ (eq. 2.1) which extends from the diode to the deep p-well, and
 150 sometimes also to the backside (in this case if one wants to collect the signal also on this electrode,
 151 additional process must be done).

²Moore's law states that logic density doubles every two years.

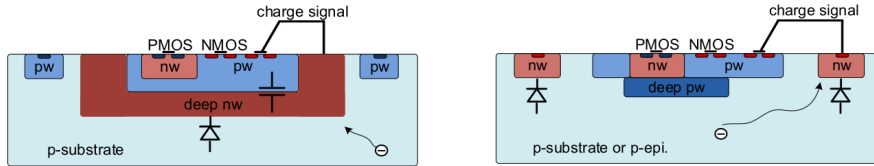


Figure 2.4: Concept cross-section with large and small fill factor

152 2.4.1 DMAPS: large and small fill factor

153 There are two different sensor-design approaches (figure 2.4) to DMAPS:

- 154 • large fill factor: a large collection electrode that is a large deep n-well and that host the
- 155 embedded electronics
- 156 • small fill factor: a small n-well is used as charge collection node

157 To implement a uniform and stronger electric field, DMAPS often uses large electrode design that
158 requires multiple wells (typically four including deep n and p wells); this layout adds on to the
159 standard terms of the total capacity of the sensor a new term (fig. 2.5), that contributes to the
160 total amplifier input capacity. In addition to the capacity between pixels (C_{pp}) and between the
161 pixel and the backside (C_b), a non-negligible contribution comes from the capacities between wells
162 (C_{WW} and C_{SW}) needed to shield the embedded electronics. These capacities affect the thermal
163 and 1/f noise of the charge amplifier and the τ_{CSA} too:

$$ENC_{thermal}^2 \propto \frac{4}{3} \frac{kT}{g_m} \frac{C_D^2}{\tau_{sh}} \quad (2.6) \quad \tau_{CSA} \propto \frac{1}{g_m} \frac{C_D}{C_f} \quad (2.7)$$

165 where g_m is the transconductance, τ_{sh} is the shaping time.

166 Among the disadvantages coming from this large input capacity could be the coupling between
167 the sensor and the electronics resulting in cross talk: noise induced by a signal on neighbouring
168 electrodes; indeed, since digital switching in the FE electronics do a lot of oscillations, this problem
169 is especially connected with the intra wells capacities. So, larger charge collection electrode

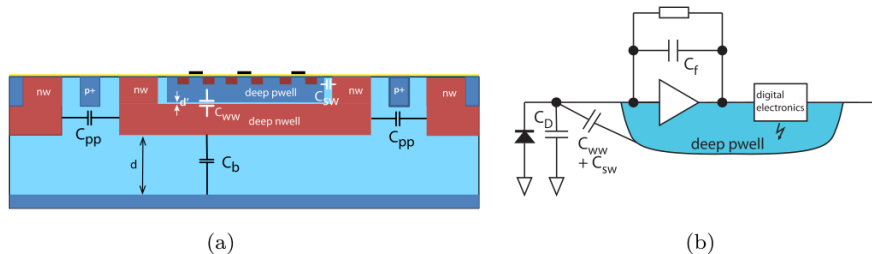


Figure 2.5: C_{pp} , C_b , C_{WW} , C_{SW}

169 sensors provide a uniform electric field in the bulk that results in short drift path and so in good
170 collection properties, especially after irradiation, when trapping probability can become an issue.
171 The drawback of a large fill-factor is the large capacity (~ 100 fF): this contributes to the noise
172 and to a speed penalty and to a larger possibility of cross talk.

173 The small fill-factor variant, instead, benefits from a small capacity (5-20 fF), but suffers from
174 a not uniform electric field and from all the issue related to that. **Ho già detto prima parlando dei
175 MAPS, devo ripetere qui?**

176 As we'll see these two different types of sensor require different amplifier: the large electrode one is
177 coupled with the charge sensitive amplifier, while the small one with voltage amplifier (sec 2.5.1).

179 2.4.2 A modified sensor

180 A process modification developed by CERN in collaboration with the foundries has become the
181 standard solution to combine the characteristics of a small fill factor sensor (small input amplifier

	small fill factor	large fill factor
small sensor C	✓ (< 5 fF)	✗ (~ 100-200 fF)
low noise	✓	✗
low cross talk	✓	✗
velocity performances	✓	✗ (~ 100 ns)
short drift paths	✗	✓
radiation hard	✗	✓

Table 2.1: Small and large fill factor DMAPS characteristics

capacity) and of large fill factor sensor (uniform electric field) is the one carried out for ALICE upgrade about ten years [1].

A compromise between the two sensors could also be making smaller pixels, but this solution requires reducing the electronic circuit area, so a completely new pixel layout should be though. The modification consists in inserting a low dose implant under the electrode and one its advantage lies in its versatility: both standard and modified sensor are often produced for testing in fact.

Before the process modification the depletion region extends below the diode towards the substrate, and it doesn't extend laterally so much even if a high bias is applied to the sensor (fig. 2.6). After, two distinct pn junctions are built: one between the deep p well and the n^- layer, and the other between the n^- and the p^- epitaxial layer, extending to the all area of the sensor. Since deep p well and the p-substrate are separated by the depletion region, the two p electrodes can be biased separately³ and this is beneficial to enhance the vertical electric field component. The doping concentration is a trimmer parameter: it must be high enough to be greater than the epitaxial layer to prevent the punchthrough between p-well and the substrate, but it must also be lower enough to allow the depletion without reaching too high bias.

2.5 Analog front end

After the creation of a signal on the electrode, the signal enters the front end circuit (fig.2.7), ready to be molded and transmitted out of chip. Low noise amplification, fast hit discrimination and an efficient, high-speed readout architecture, consuming as low power as possible must be provided by the readout integrated electronics (ROIC).

Let's take a look to the main steps of the analog front end chain: the preamplifier (that actually often is the only amplification stage) with a reset to the baseline mechanism and a leakage current compensation, a shaper (a band-pass filter) and finally a discriminator. The whole chain must be optimized and tuned to improve the S/N ratio: it is very important both not to have a large noise before the amplification stage in order to not multiply that noise, and chose a reasonable threshold of the discriminator to cut noise-hits much as possible.

2.5.1 Preamplifier

Even if circuits on the silicon crystal are only constructed by CMOS, a preamplifier can be modeled as an operational amplifier (OpAmp) where the gain is determined by the input and feedback impedance (first step in figure 2.7):

$$G = \frac{v_{out}}{v_{in}} = \frac{Z_f}{Z_{in}} \quad (2.8)$$

Depending on whether a capacity or a resistance is used as feedback, respectively a charge or a voltage amplifier is used: if the voltage input signal is large enough and have a sharp rise time, the voltage sensitive preamplifier is preferred. Consequently, this flavor doesn't suit to large fill factor MAPS whose signal is already enough high: $v_{in} = Q/C_D \approx 3fC/100 \text{ pF} = 0.03 \text{ mV}$, but it's fine for the small fill factor ones: $v_{in} = Q/C_D \approx 3fC/3 \text{ pF} = 1 \text{ mV}$.

In the case of a resistor feedback, if the signal duration time is longer than the discharge time ($\tau = R_S C_D$) of the detector the system works as current amplifier, as the signal is immediately

³This is true in general, but it can be denied if other doping characteristics are implemented, and we'll see that this is the case of TJ-Monopix1

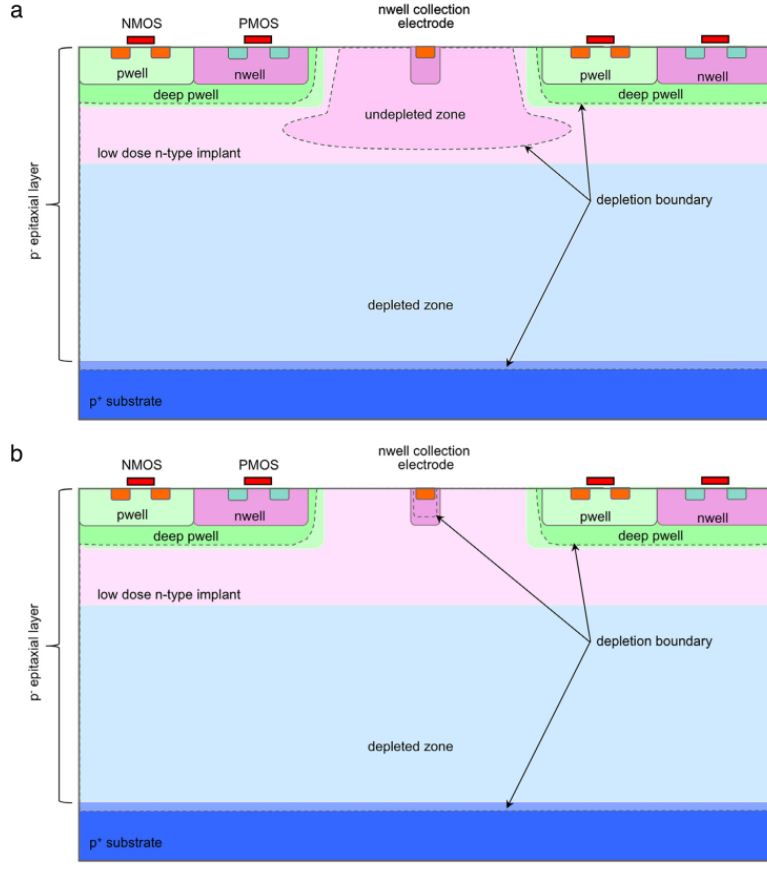


Figure 2.6: A modified process for ALICE tracker detector: a low dose n implant is used to create a planar junction. In (a) the depletion is partial, while in (b) the pixel is fully depleted.

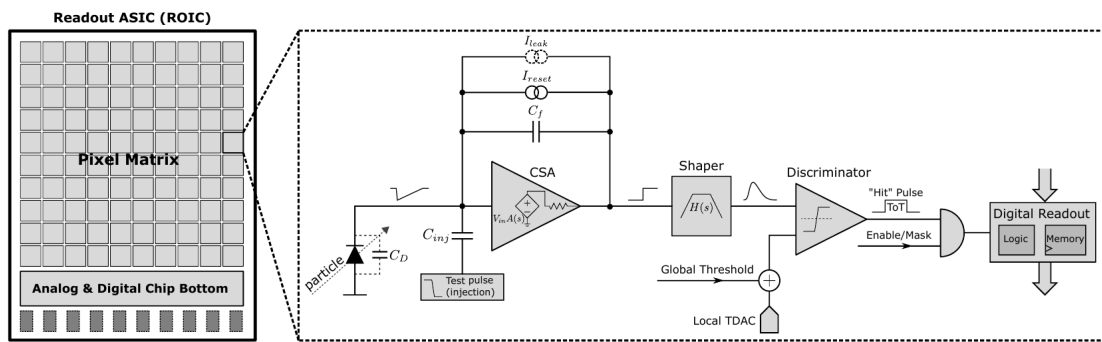


Figure 2.7: Readout FE scheme: in this example the preamplifier is a charge sensitive one (CSA) but changing the capacitive feedback into a resistive one, this can be converted in a voltage or current amplifier.

219 trasmit to the amplifier; in the complementary case (signal duration longer than the discharge
 220 time) the system integrates the current on the C_D and operates as a voltage amplifier.

221 2.6 Readout logic

222 Readout logic includes the part of the circuit which takes the FE output signal, processes it and
 223 then transmit it out of pixel and/or out of chip; depending on the situation of usage different
 224 readout characteristics must be provided.

225 To store the analogical information (i.e. charge collected, evolution of signal in time, ...) big buffers
 226 and a large bandwidth are needed; the problem that doesn't occur, or better occur only with really
 227 high rate, if one wants record only digital data (if one pixel is hit 1 is recorded, and if not 0 is
 228 recorded).

229 A common compromise often made is to save the time over threshold (ToT) of the pulse in clock
 230 cycle counts; this needs of relatively coarse requirement as ToT could be trimmer to be a dozen
 231 bits but, being correlated and hopefully being linear with the deposited charge by the impinging
 232 particle in the detector, it provides a sufficient information. The ToT digitalization usually takes
 233 advantage of the distribution of a clock (namely BCID, bunch crossing identification) on the pixels' matrix.
 234 The required timing precision is at least around 25 ns, that corresponds to the period of
 235 bunch collisions at LHC; for such reason a reasonable BCID-clock frequency for pixels detector is
 236 40 MHz.

237 Leading and trailing edges' timestamp of the pulse are saved on pixel within a RAM until they
 have been read, and then the ToT is obtained from their difference.

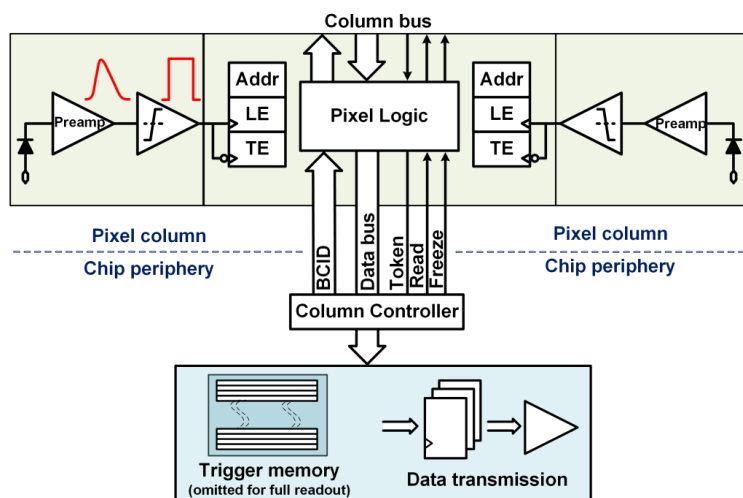


Figure 2.8: Column drain R/O scheme where ToT is saved

238 Moreover, the readout architecture can be full, if every hit is read, or triggered, if a trigger
 239 system decides if the hit must be store or not. On one hand the triggered-readout needs buffers
 240 and storage memories, on the other the full readout, because there is no need to store hit data on
 241 chip, needs an high enough bandwidth.

242 A triggered readout is fundamental in accelerator experiments where the quantity of data to store
 243 is too large to be handled, and some selections have to be applied by the trigger: to give an order
 244 of growth, at LHC more than 100 TBit/s of data are produced, but the storage limit is about 100
 245 MBit/s [2] (pag. 797).

246 Typically the trigger signal is processed in a few μs , so the pixel gets it only after a hundred clock
 247 cycles from the hit arrival time: the buffer depth must than handle the higher trigger latency.

248 After having taken out the data from the pixel, it has to be transmitted to the end of column
 249 (EoC) where a serializer deliver it out of chip, typically to an FPGA.

250 There are several ways of transmitting data from pixel to the end of column: one of the most
 251 famous is the column-drain read out, developed for CMS and ATLAS experiments [3]. All the
 252 pixels in a double-column share a data bus and only one pixel at a time, according to a priority
 253 chain, can be read. The reading order circuit is implemented by shift register (SR): when a hit

arrives, the corresponding data, which can be made of timestamp and ToT, is temporarily stored on a RAM until the SH does not allow the access to memory by data bus.
Even if many readout architectures are based the column-drain one, it doesn't suit for large size matrices. The problem is that increasing the pixels on a column would also raise the number of pixels in the priority chain and that would result in a slowdown of the readout.

If there isn't any storage memory, the double-column behaves as a single server queue and the probability for a pixel of waiting a time T greater than t , with an input hit rate on the column μ and an output bandwidth B_W is [4]:

$$P(T > t) = \frac{\mu}{B_W} e^{-(B_W - \mu)t} \quad (2.9)$$

To avoid hit loss (let's neglect the contribution to the inefficiency of the dead time τ due to the AFE), for example imposing $P(T > t) \sim 0.001$, one obtains $(B_W - \mu) t_t \sim 6$, where t_t is the time needed to transfer the hit; since t_t is small, one must have $B_W \gg \mu$, that means a high bandwidth [4].

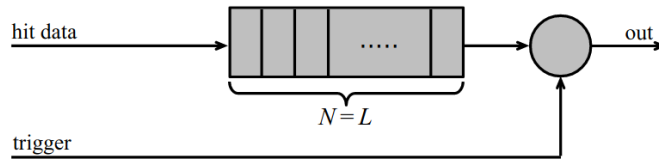


Figure 2.9: Block diagram of a pipeline buffer: N is the dimension of memory buffer and L is the trigger latency expressed in BCID cycles

Actually the previous one is an approximation since each pixel sees a different bandwidth depending on the position on the queue: the first one sees a full bandwidth, but the next sees a smaller one because occasionally it can be blocked by the previous pixel. Then the bandwidth seen by the pixel i is $B_i = B - \sum_j \mu_j$, where μ_j is the hit rate of the j th pixel.
The efficiency requirement on the bandwidth and the hit rate becomes: $B_{W,i} > \mu_i$, where the index i means the constraint is for a single pixel; if all the N pixels on a column have the same rate $\mu = N\mu_i$, the condition reduces to $B_W > \mu$. The bandwidth must be chosen such that the mean time between hits of the last pixel in the readout chain is bigger than that.

In order to reduce the bandwidth a readout with zero suppression on pixel is typically employed; this means that only information from channels where the signal exceeds the discriminator threshold are stored. Qualscosa sulla zero suppression? La metto qui questa affermazione?

If instead there is a local storage until a trigger signal arrives, the input rate to column bus μ' is reduced compared to the hit rate μ as: $\mu' = \mu \times r \times t$, where r is the trigger rate and t is the bunch crossing period. In this situation there is a more relaxed constraint on the bandwidth, but the limiting factor is the buffer depth: the amount of memory designed depends both on the expected rate μ and on the trigger latency t as $\propto \mu \times t$, that means that the higher the trigger latency and the lower the hit rate to cope with.

In order to have an efficient usage of memory on pixels' area it's convenient grouping pixels into regions with shared storage. Let's compare two different situations: in the first one a buffer is located on each pixel area, while in the second one a core of four pixels share a common buffer (this architecture is commonly called FE-I4).

Consider a 50 kHz single pixel hits rate and a trigger latency of 5 μs , the probability of losing hits is:

$$P(N > 1|\nu) = 1 - P(N = 0|\nu) - P(N = 1|\nu) = 1 - e^{-\nu}(1 + \nu) \approx 2.6\% \quad (2.10)$$

where I have assumed a Poissonian distribution with mean $\nu = 0.25$ to describe the counts N . To get an efficiency ϵ greater than 99.9 % a 3 hit depth buffer is needed:

$$P(N > 3|\nu) = 1 - \sum_{i=0}^3 P(N = i|\nu) < 0.1\% \quad (2.11)$$

Considering the second situation: if the average single pixel rate is still 50 kHz, grouping four pixels the mean number of hits per trigger latency is $\nu = 0.25 \times 4 = 1$. To get an efficiency of 99.9% (eq. 2.11) a buffer depth of 5 hits in the four-pixels region, instead of 3 per pixels, is needed.

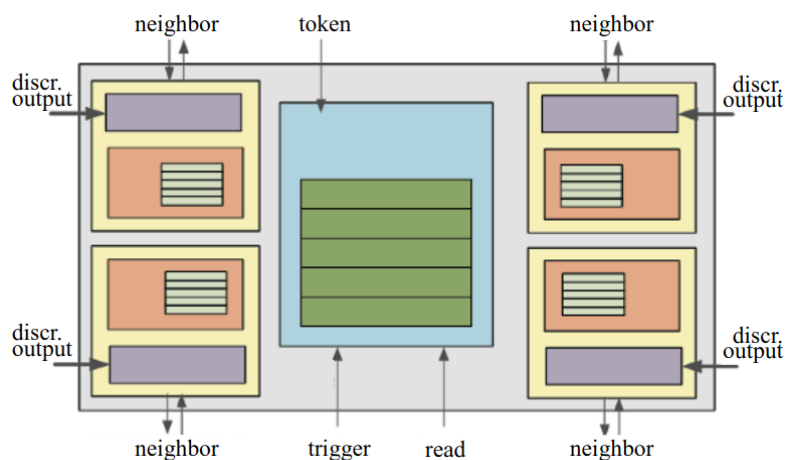


Figure 2.10: Block diagram of the FE-I4 R/O. Read and memory management section is highlighted in light blue; latency counters and trigger management section are highlighted in green; hit processing blocks are highlighted in purple; ToT counters and ToT management units are highlighted in orange

²⁹⁵ **Chapter 3**

²⁹⁶ **Use of pixel detectors**

²⁹⁷ There always was a tight relation between the development of cameras and pixel detectors since
²⁹⁸ 1969, when the idea of CCDs, thanks to whom Boyle and Smith were awarded the Nobel Prize in
²⁹⁹ Physics in 2009, revolutionized photography allowing light to be captured electronically instead of
³⁰⁰ on film. Even though the CMOS technology was already known when CCDs spread, the costs of
³⁰¹ productions were too high to allow the diffusion of these sensors for which needed to wait until
³⁰² 1990s. From that period on, the fast diffusion of CMOS was mainly due to the less cost than CCD,
³⁰³ and the less power required for supply.

³⁰⁴ The principal use cases of pixel detectors are particle tracking and imaging: in the former case
³⁰⁵ individual charged particles have to be identified, in the latter instead an image is obtained by
³⁰⁶ the usually un-triggered accumulation of the impinging radiation. Also the demands on detectors
³⁰⁷ performance depends on their usage, in particular tracking requires high spatial resolution, fast
³⁰⁸ readout and radiation hardness.

³⁰⁹ For scientific imaging, instead, the applications vary from astrophysics and medical imaging
³¹⁰ to studies of protein dynamics, *altro?* and art authentication, for example. The counting mode
³¹¹ represents the principal imaging technique, a direct

³¹² **3.1 Tracking in HEP**

³¹³ Historically, the first pixel detector employed in particle physics was a CCD: it was installed in
³¹⁴ the spectrometer at the CERN's Super Proton Synchrotron (SPS) by the ACCMOR Collaboration
³¹⁵ (Amsterdam, CERN, Cracow, Munich, Oxford, RAL) at mid 1980s, with the purpose of studying
³¹⁶ the recently-discovered charm particles. The second famous usage of CCDs took place at SLAC
³¹⁷ in the Large Detector (SLD) during the two years 1996-98. From that period on particle tracking
³¹⁸ in experiments have been transformed radically: it was mandatory for HEP experiments to build
³¹⁹ an inner vertex detector. In 1991, the more demanding environments led to the development of hy-
³²⁰ brid pixel detectors: a dedicated collaboration, RD19, was established at CERN with the specific
³²¹ goal to define a semiconductor micropattern detector with an incorporated signal processing at a
³²² microscopic level. In those years a wide set of prototypes of hybrid pixel has been manufactured;
³²³ among the greatest productions a mention goes to the huge ATLAS and CMS vertex detectors.
³²⁴ From the middle of 2013 a second collaboration, RD 53, has been established with the new goal
³²⁵ to find a pixel detector suitable for phase II future upgrades of those experiments. Even if the col-
³²⁶ laboration is specifically focused on design of hybrid pixel readout chips (aiming to 65 nm technique
³²⁷ so that the electronics fits within the pixel area), also other options have been taken in account
³²⁸ and many test have been done on MAPS for example. Requirements imposed by HL-LHC will
³²⁹ become tighter in time: for example, a dose and radiation of 5 Mrad and 1016NIEL are expected
³³⁰ after 5 years of operation. Time resolution, material budget and power consumption are also issues
³³¹ for the upgrade: a time resolution better than 25 ns for a bunch crossing frequency of 40 MHz, a
³³² material budget lower than 2% and a power consumption lower than 500 mW/cm² are required.

³³³ Amidst the solutions proposed 3D silicon detector, invented by Sherwood Parker in 1995, and
³³⁴ MAPS are the most promising. In 3D sensors the electrode is a narrow column of n-type implanted
³³⁵ vertically across the bulk instead of being implanted on the wafer's surface. The charge produced
³³⁶ by the impinging particle is then drifted transversally within the pixel, and, as the mean path
³³⁷ between two electrode can be sufficiently low, the trap probability is not an issue. 3D pixels have

338 been already proved in ATLAS tracker qualcosa? tipo anno e rif a caso. Even if 3D detector are
339 adequately radiation hard, MAPS architecture looked very promising from the beginning: they
340 overcome both the CCDs long reading time and the hybrid problems (I have already explained
341 in section ?? the benefits of MAPS). Experiments such as ALICE at LHC and STAR at RHIC
342 have already introduced the CMOS MAPS technology in their detectors. ALICE Tracking System
343 (ITS2), upgraded during the LHC long shut down in 2019-20, was the first large-area ($\sim 10 \text{ m}^2$
344 covered by 2.5 Gpixels) silicon vertex detector based on CMOS MAPS.

345 3.1.1 Hybrid pixels at LHC: ATLAS, CMS and LHC-b

346 ATLAS

347 ATLAS is one of two general-purpose detectors at the LHC and has the largest volume detector ever
348 constructed for a particle collider (46 m long and 25 m in diameter). The inner detector consists
349 of three different systems all immersed in a magnetic field parallel to the beam axis. The main
350 components of the Inner Detector are: the pixel, the micro-strips and transition radiation trackers.
351 92 million pixels are divided in 4 barrel layers and 3 disks in each end-cap region, covering a total
352 area of 1.9 m^2 and having a 15 kW of power consumption.

353 As stated by the ATLAS collaboration the pixel detector is exposed by an extreme particle flux:
354 "By the end of Run 3¹, the number of particles that will have hit the innermost pixel layers will
355 be comparable to the number it would receive if it were placed only a few kilometres from the Sun
356 during a solar flare". And the particle density will increase even more with HL-LHC. The most
357 ambitious goal is employ a MAPS-based detector for the inner-layer barrels, and for this reason
358 the RD53 collaboration is performing many test on MAPS prototypes, as Monopix of which I will
359 talk about in section ??.

360 Up to now this possibility will be eventually implemented during the second phase of the HL-
361 LHC era, as at the start of high-luminosity operation the selected option is the hybrid one. The
362 sensor, which is not selected yet, will be bonded with ITkPix, the first full-scale 65 nm hybrid
363 pixel-readout chip and is developed by the RD53 collaboration. For the sensor a valuable option
364 is using 3D pixels, which have already proved themselves in ATLAS, for the insertable B layer
365 (IBL).qualcosa sui 3d usati a ATLAS. These pixel tracking systems will increase the number of
366 pixels of a factor about 7, passing from 92 milioni to 6 miliardi.

367 CMS

368

369 LHCb

370 LHCb is a dedicated heavy-flavour physics experiment by exploiting pp interactions at 14 TeV at
371 LHC. It was the last experiment to upgrade the vertex detector Vertex Locator (VELO) replacing
372 the silicon-strip with pixels in May 2022. As the instantaneous luminosity in Run3 is increased by a
373 factor $\lesssim 10$, much of the readout electronics and of the trigger system have been developed in order
374 to cope with the large interaction rate. To place the detector as close as possible to the beampipe
375 and reach a better track reconstruction resolution, the VELO can be moved: during the injection of
376 LHC protons it is parked at 3 cm from the beams and only when the stability is reached it is brought
377 at ~ 5 mm. Radiation hardness as well as readout speed are then a priority for the detectors:
378 that's why the collaboration opted for a hybrid system. The VeloPix is made bonding sensors,
379 each measuring 55×55 micrometers, 200 μm -thick to a 200 μm -thick ASIC specially developed for
380 LHCb and coming from the Medipix family (sec. ??). It is capable of handling up to 900 million
381 hits per second per chip, while withstanding the intense radiation environment. The new VeloPix
382 readout chips have a readout speeds of up to 20 Gb/s each, resulting in 3 Tb/s torrent of data
383 Since the detector is operated under vacuum near the beam pipe, the heat removal is particularly
384 difficult and evaporative CO₂ microchannel cooling are used.

¹Run 3 start in June 2022

385 **3.1.2 A DEPFET example: Belle-II**

386 **3.1.3 CMOS MAPS: ALICE and STAR**

387 **ALICE**

388 ALICE (A Large Ion Collider Experiment) is a detector dedicated to heavy-ion physics and to the
389 study of the condensed phase of the chromodynamics at the LHC. The tracking detector consists of
390 the Inner Tracking System (ITS), the gaseous Time Projection Chamber (TPC) and the Transition
391 Radiation Detector (TRD) and those are embedded in a magnetic field of 0.5 T. The ITS is made
392 by six layers of detectors, two for each type, from the interaction point outwards: Silicon Pixel
393 Detector (SPD), Silicon Drift Detector (SDD) and Silicon Strip Detector (SSD). Contrary to the
394 others LHC experiments, ALICE tracker is placed in a quite different environments: the expected
395 dose is smaller by two order of magnitude and the rate of interactions is few MHz instead of
396 40 MHz, but the number of particles comes out of each interaction is higher (the SPS is invested
397 by a density of particles of $\sim 100 \text{ fm}^{-3}$). The reconstruction of very complicated events with a
398 large number of particle is a challenge, hence to segment and to minimize the amount of material,
399 which may cause secondary interaction complicating further the event topology, is considered a
400 viable strategy.

401 **Upgrade con Monopix1** Thanks to the reduction of the material budget, ITS2, which uses
402 the ALPIDE chip developed by ALICE collaboration, obtained an amazing improvement both
403 in the position measurement and in the momentum resolution, improving the efficiency of track
404 reconstruction for particle with very low transverse momentum (by a factor 6 at $pT \sim 0.1 \text{ GeV}/c$).
405 Further advancements in CMOS MAPS technology are being aggressively pursued for the ALICE
406 ITS3 vertex detector upgrades (foreseen around 2026-27), with the goals of further reducing the
407 sensor thickness and improving the readout speed of the devices, while keeping power consumption
408 at a minimum. **STAR**

409 MIMOSA-28 devices for the first MAPS-based vertex detector: a 356 Mpixel two-layer barrel
410 system for the STAR experiment at Brookhaven's Relativistic Heavy Ion Collide

411 **3.2 Application in imaging**

412 **3.2.1 Medipix**

413 Medipix is a family of read-out chips for particle imaging and detection developed by the Medipix
414 Collaborations. The original concept is that it works like a camera, detecting and counting each in-
415 dividual particle hitting the pixels when its electronic shutter is open. This enables high-resolution,
416 high-contrast, noise hit free images - making it unique for imaging applications. Medipix2 collabora-
417 tion was started in 1999, the Medipix3 collaboration in 2005 and finally the Medipix4 collaboration
418 in 2016. In generale essendo single photon counting ci sono un sacco di applicazioni: fai un elenco.

419 Dalla collaborazione Medipix2 è nato anche il chip Timepix

420 Medipix2 250 mm CMOS process

421 Medipix3 chip in 130nm CMOS.

422 The aim of the Medipix4 collaboration is designing pixel read-out chips that for the first time
423 are fully prepared for TSV processing and may be tiled on all four sides. Two new chips are
424 foreseen: Medipix4, which will target spectroscopic X-ray imaging at rates compatible with medical
425 CT scans, and Timepix4, which will provide particle identification and tracking with higher spatial
426 and timing precision.

427 Utilizzati in medicina: Radiography and computed tomography (CT) use X-ray photons to study
428 the human body. The Medipix chips that implement on-pixel single photon counting provide many
429 advantages for use in these fields. The technology has been applied in X-ray CT, in prototype
430 systems for digital mammography, in CT imagers for mammography and for beta- and gamma-
431 autoradiography of biological samples. , the images are no longer black and white

432 Timepix is being exploited for radiation monitoring in NASA's Orion rocket and at the Inter-
433 national Space Station.

434 As an example, the chips are now being used in the ATLAS experiment to provide independent,
435 real-time information about the radiation environment in the experimental cavern - in principle the
436 same task that Timepix does at the International Space Station. A direct 'spin back' to high-energy
437 physics is VELOpix, based on Timepix3. Benefiting from developments made in the framework

⁴³⁸ of the Medipix3 consortium which were not originally intended for high-energy physics, VELOpix
⁴³⁹ will serve as the read-out chip in the new vertex detector of the LHCb experiment, which is planned
⁴⁴⁰ for installation in 2018.

⁴⁴¹ **3.2.2 Applicability to FLASH radiotherapy**

⁴⁴² **Chapter 4**

⁴⁴³ **TJ-Monopix1**

⁴⁴⁴ TJ-Monopix1 is a small electrode DMAPS with fast R/O capability, fabricated by TowerJazz
⁴⁴⁵ foundry in 180 nm CMOS imaging process. It is part, together with prototypes from other series
⁴⁴⁶ such as TJ-MALTA, of the ongoing R&D efforts aimed at developing DMAPS in commercial CMOS
⁴⁴⁷ processes, that could cope with the requirements at accelerator experiments. Both TJ-Monopix
⁴⁴⁸ and TJ-MALTA series [5], produced with the same technology by TowerJazz (the timeline of the
⁴⁴⁹ foundry products is shown in figure 4.1), are small electrode demonstrators and principally differ in
⁴⁵⁰ the readout design: while Monopix implements a column-drain R/O, an asynchronous R/O without
⁴⁵¹ any distribution of BCID has been used by TJ-Malta in order to reduce power consumption.



Figure 4.1: Timeline in TowerJazz productions in 180 nm CMOS imaging process

⁴⁵² Another Monopix series, but in 150 nm CMOS technology, has been produced by LFoundry [6].
⁴⁵³ The main differences between the LF-Monopix1 and the TJ-Monopix1 (summarized in table 4.2),
⁴⁵⁴ lay in the sensor rather than in the readout architecture, as both chips implements a fast col-
⁴⁵⁵ umn drain R/O with ToT capability [7][8]. Concerning the sensors, either are based on a p-type
⁴⁵⁶ substrate, but with slightly different resistivities; in addition LFoundry pixels are larger, thicker
⁴⁵⁷ and have a large fill factor (the very deep n-well covers ~55% of the pixel area). The primary
⁴⁵⁸ consequence is that LF-Monopix1 pixels have a higher capacity resulting in higher consumption
⁴⁵⁹ and noise. As I discussed in section 2.4.1, the fact that LF-Monopix has a large fill factor electrode
⁴⁶⁰ is expected to improve its radiation hardness. Indeed, a comparison of the performance of the
⁴⁶¹ two chips showed that TJ-Monopix suffers a comparatively larger degradation of efficiency after
⁴⁶² irradiation, due to the low electric field in the pixel corner; on the other hand, a drawback of the
⁴⁶³ large fill factor in LF-Monopix is a significant cross-talk.

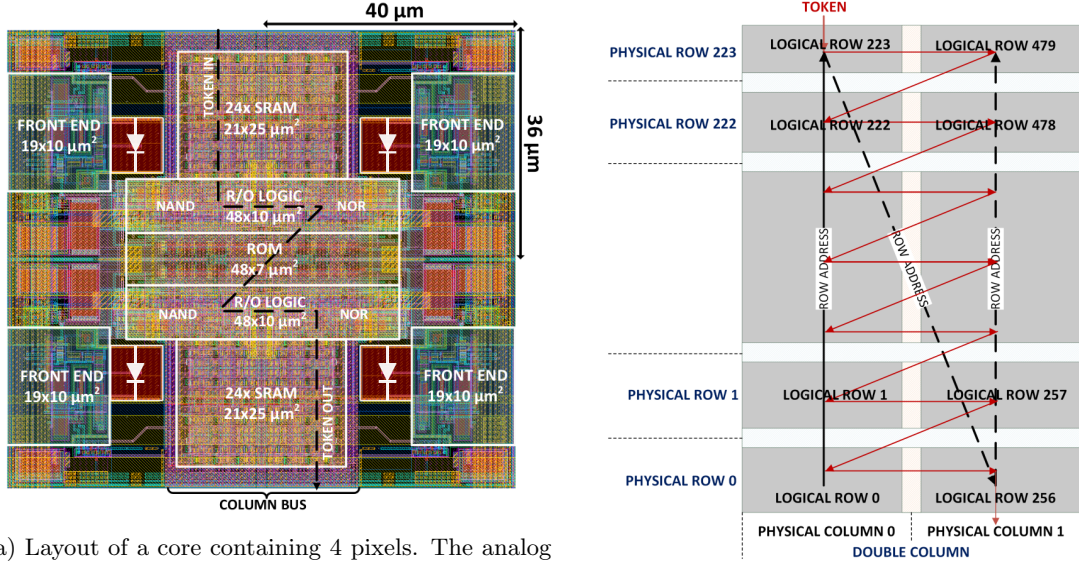
⁴⁶⁴ The TJ-Monopix1 chip contains, apart from the pixels matrix, all the required support blocks
⁴⁶⁵ used for configuration and testing:

- ⁴⁶⁶ the whole matrix contains 224×448 pixels, yielding a total active area approximately equal
⁴⁶⁷ to 145 mm^2 over a total area of $1 \times 2 \text{ cm}^2$;
- ⁴⁶⁸ at the chip periphery are placed some 7-bit Digital to Analog Converter (DAC), used to
⁴⁶⁹ generate the analog bias voltage and current levels and to configure the FE;

	LF-Monopix1	TJ-Monopix1
Resistivity	$>2\text{ k}\Omega\text{cm}$	$>1\text{ k}\Omega\text{cm}$
Pixel size	$50 \times 250\mu\text{m}^2$	$36 \times 40\mu\text{m}^2$
Depth	$100\text{-}750\mu\text{m}$	$25\mu\text{m}$
Capacity	$\sim 400\text{ fF}$	$\sim 3\text{ fF}$
Preamplifier	charge	voltage
Threshold trimming	on pixel (4-bit DAC)	global threshold
ToT	8 bits	6 bits
Consumption	$\sim 300\text{ mW/cm}^2$	$\sim 120\text{ mW/cm}^2$
Threshold	$1500 e^-$	$\sim 270 e^-$
ENC	$100 e^-$	$\sim 30 e^-$

Table 4.1: Main characteristics of Monopix1 produced by TowerJazz and LFoundry [7][8]

- 470 • at the EoC is placed a serializer to transferred datas immediately, indeed no trigger memory
 471 is implemented in this prototypes;
- 472 • the matrix power pads are distributed at the sides
- 473 • four pixels which have analog output and which can be monitored with an oscilloscope, and
 474 therefore used for testing
- 475 Pixels are grouped in 2×2 cores (fig. 4.2a): this layout allows to separate the analog and the
 476 digital electronics area in order to reduce the possible interference between the two parts. In
 477 addition it simplifies the routing of data as pixels on double column share the same column-bus to
 478 EoC. Therefore pixels can be addressed through the physical column/row or through the logical
 479 column/row, as shown in fig. 4.2b: in figure is also highlighted the token propagation path, whose
 480 I will discuss later.



(a) Layout of a core containing 4 pixels. The analog FE and the digital part are separated in order to reduce cross-talk be

(b)

4.1 The sensor

481 As already anticipated, TJ-Monopix1 has a p-type epitaxial layer and a n doped small collection
 482 electrode ($2\mu\text{m}$ in diameter); to avoid the n-wells housing the PMOS transistors competing for the
 483 charge collection, a deep p-well substrate, common to all the pixel FE area, is used. TJ-Monopix1
 484 adopts the modification described in section 2.4.2 that allows to achieve a planar depletion region
 485

Parameter	Value
Matrix size	$1 \times 2 \text{ cm}^2$
Pixel size	$36 \times 40 \mu\text{m}^2$
Depth	$25 \mu\text{m}$
Electrode size	$2 \mu\text{m}$
BCID	40 MHz
ToT-bit	6
Power consumption	$\sim 120 \text{ mW/cm}^2$

Table 4.2

near the electrode applying a relatively small reverse bias voltage. This modification improves the efficiency of the detector, especially after irradiation, however a simulation of the electric field in the sensor, made with the software TCAD (Technology Computer Aided Design), shows that a nonuniform field is still produced in the lateral regions of the pixel compromising the efficiency at the corner. Two variations to the process have been proposed in order to further enhance the transversal component of electric field at the pixel borders: on a sample of chip, which includes the one in Pisa, a portion of low dose implant has been removed, creating a step discontinuity in the deep p-well corner (fig. 4.3); the second solution proposed[MOUSTAKAS THESYS, PAG 58] consists in adding an extra deep p-well near the pixel edge. A side effect of the alteration in the low dose implant is that the separation between the deep p-well and the p-substrate becomes weak to the point that they cannot be biased separately to prevent the punchthrough.

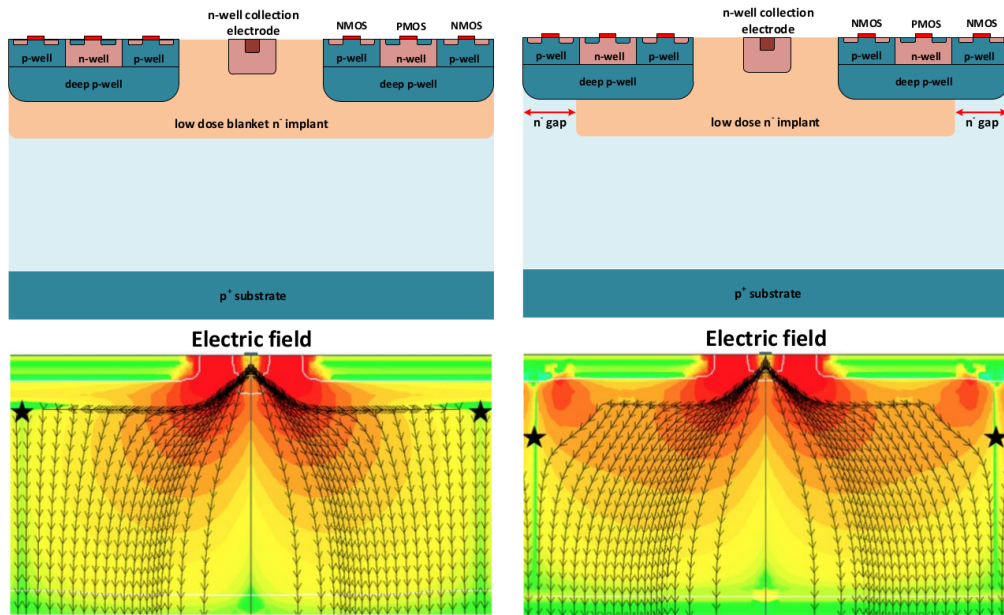


Figure 4.3: (a) The cross-section of a monolithic pixel in the TJ-Monopix with modified process; additionally in (b) a gap in the low dose implant is created to improve the collection of charge due to a bigger lateral component of the electric field. this point in figure is indicated by a star . transversal component of the electric field drops at the pixel corner

Moreover, to investigate the charge collection properties, pixels within the matrix are split between bottom top half and bottom half and feature a variation in the coverage of the deep p-well: the electronics area can be fully covered or not. In particular the pixels belonging to rows from 0 to 111 are fully covered (FDPW) and pixels belonging to rows from 112 to 223 have a reduced p-well (RDPW), resulting in a enhancement of the lateral component of the electric field.

502 4.2 Front end

503 The matrix is split in four sections, each one corresponding to a different flavor of the FE. The
504 four variation have been implemented in order to test the data-bus readout circuits and the input
reset modes.

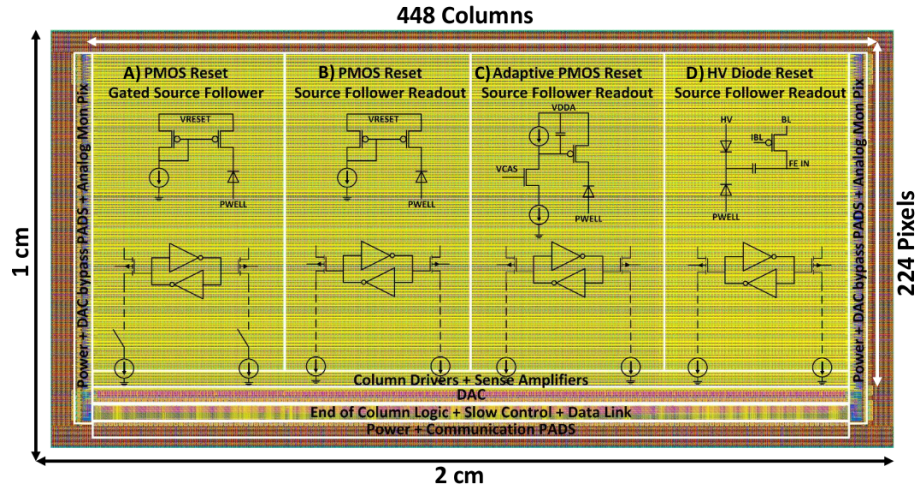


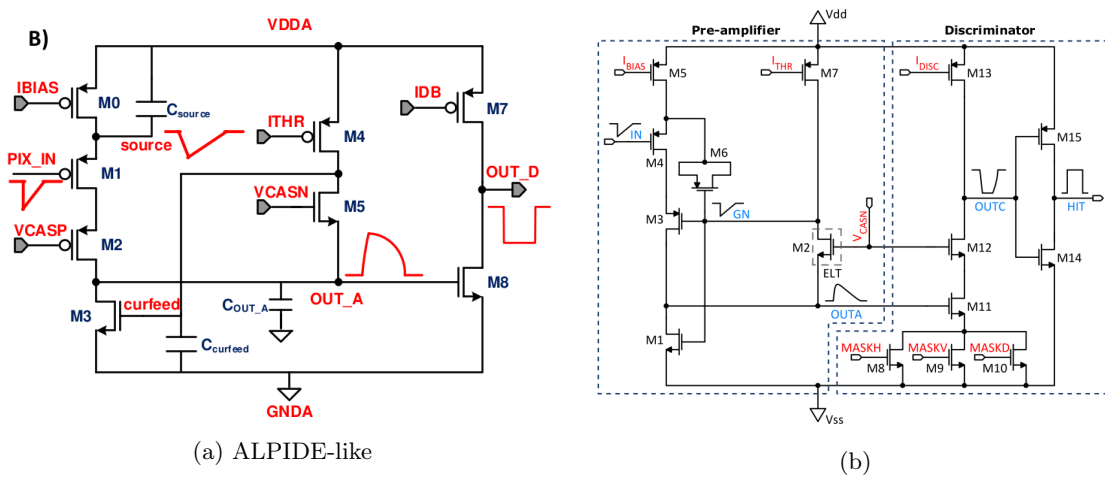
Figure 4.4

505 All the flavors implement a source-follower double-column bus readout: the standard variation
 506 is the flavor B, that features a PMOS input reset (referred as "PMOS reset"). Flavor A is identical
 507 to flavor B except for the realization of the source follower (it is a gated one) that aim to reduce
 508 the power consumption.[cosa significa?](#) C instead implements a novel leakage compensation circuit.
 509 Moreover the collection electrode in flavors A, B, C is DC-coupled to the front-end input, while
 510 in D is AC-coupled, providing to apply a high bias voltage; for this reason flavor D is called "HV
 511 flavor".

513 R resistenza di reset deve essere abbastanza grande in modo da far sì che il ritorno allo zero
514 è abbastanza lento (non devi "interferire" con la tot slope e non devi più corto del tempo del
515 preamplificatore, sennò hai perdita di segnale). Baseline reset: all'input solitamente hai un PMOSS
516 o un diodo; R reset; Voltage amplifier

517 4.2.1 ALPIDE-like

518 ALPIDE chips, developed by the ALICE collaboration, implemented a standard FE to the point
 519 that many CMOS MAPS detectors used a similar FE and are called "ALPIDE-like". Considering
 520 that both TJ-Monopix1 and ARCADIA-MD1 have an ALPIDE-like FE, I am going to explain the
 broad principles of the early FE stage. The general idea is of the amplification to transfer the



522 charge from a bigger capacity[9], C_{source} , to a smaller one, C_{out} : the input transistor M1 with
 523 current source IBIAS acts as a source follower and this forces the source of M1 to be equal to the
 524 gate input $\Delta V_{PIX_IN} = Q_{IN}/C_{IN}$.

$$Q_{source} = C_{source} \Delta V_{PIX_IN} \quad (4.1)$$

525 The current in M2 and the charge accumulates on C_{out} is fixed by the one on C_{source} :

$$\Delta V_{OUT_A} = \frac{Q_{source}}{C_{OUT_A}} = \frac{C_{source} \Delta V_{PIX_IN}}{C_{OUT_A}} = \frac{C_{source}}{C_{OUT_A}} \frac{Q_{IN}}{C_{IN}} \quad (4.2)$$

526 A second branch (M4, M5) is used to generate a low frequency feedback, where VCASN and ITHR
 527 set the baseline value of the signal on C_{OUT_A} and the velocity to goes down to the baseline.

IL RUOLO DI CURVFEED NON L'HO CAPITO.

529 Finally IDB defines the charge threshold with which the signal OUT_A must be compared: de-
 530 pending on if the signal is higher than the threshold or not, the OUT_D is high or low respectively.

531 The actual circuit implemented in TJ-Monopix1 is shown in figure 4.5b: the principal difference
 532 lays in the addition of disableing pixels' readout. This possibility is uttermost important in order to
 533 reduce the hit rate and to avoid saturating the bandwidth due to the noisy pixels, which typically
 534 are those with manufacturing defects. In the circuit transistors M8, M9 and M10 have the function
 535 of disabling registers with coordinates MASKH, MASKV and MASKD (respectively vertical, ori-
 536 ginal and diagonal) from readout: if all three transistors-signals are low, the pixel's discriminator
 537 is disabled. Compared with a configurable masking register which would allow disableing pixels
 538 individually, to use a triple redundancy reduces the sensistivity to SEU¹ but also gives amount of
 539 intentionally masked ("ghost") pixels. This approach is suitable only for extremely small number
 540 N of pixel has to be masked: if two coordinate projection scheme had been implemented, the
 541 number of ghost pixels would have scale with N^2 , if instead three coordinates are used, the N's
 exponential is lower than 2 (fig. 4.6)

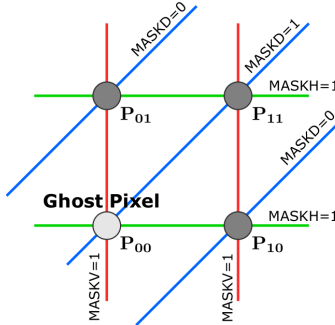


Figure 4.6

542

4.3 Readout logic

544 The simplest readout is "rolling shutter", in which peripheral logic along the chip edge addresses
 545 rows in turn, and analogue signals are transmitted by column lines to peripheral logic at the
 546 bottom of the imaging area. TJ-Monopix1 has a triggerless, fast and with ToT capability R/O
 547 which is based on a column-drain architecture. On the pixel are located two Random Access
 548 Memory (RAM) cells to store the 6-bit LE and 6-bit TE of the pulse, and a Read-Only Memory
 549 (ROM) containing the 9-bit pixel address. Excluded these memories, TJ-Monopix1 hasn't any
 550 other buffer: if a hit arrives while the pixel is already storing a previous one, the new data get lost.

¹Single Event Upset, in sostanza è quando un bit ti cambia valore (da 0 a 1 o viceversa) perché una particella deposita carica nell'elettronica che fa da memoria registro/RAM/.... Questo tipo di elettronica ha bisogno di un sacco di carica prima che il bit si "fippi" (cambi valore), infatti tipicamente per avere un SEU non basta una MIP che attraversa esattamente quel pezzo di chip in cui è implementata la memoria, ma un adrone che faccia interazione nucleare producendo più carica di quanto farebbe una MIP. Questo metodo pur essendo più comodo richiede less amount of area ha però come drawback che il registro può essere soggetto a SEU problema non trascurabile in acceleratori come HL-LHC adronici

Parameter	Meaning	
IBIAS	sets the discriminator threshold	yes
IDB	sets the velocity of the return to the baseline	yes
ITHR	sets the baseline of the signal	yes
ICASN	sets the gain of the preamplifier	yes
VRESET	sets the gain of the preamplifier	yes
IRESET	sets the gain of the preamplifier	no

Table 4.3: FE parameters which must be setted through the DAQ. "Function" means that higher parameter implies higher value

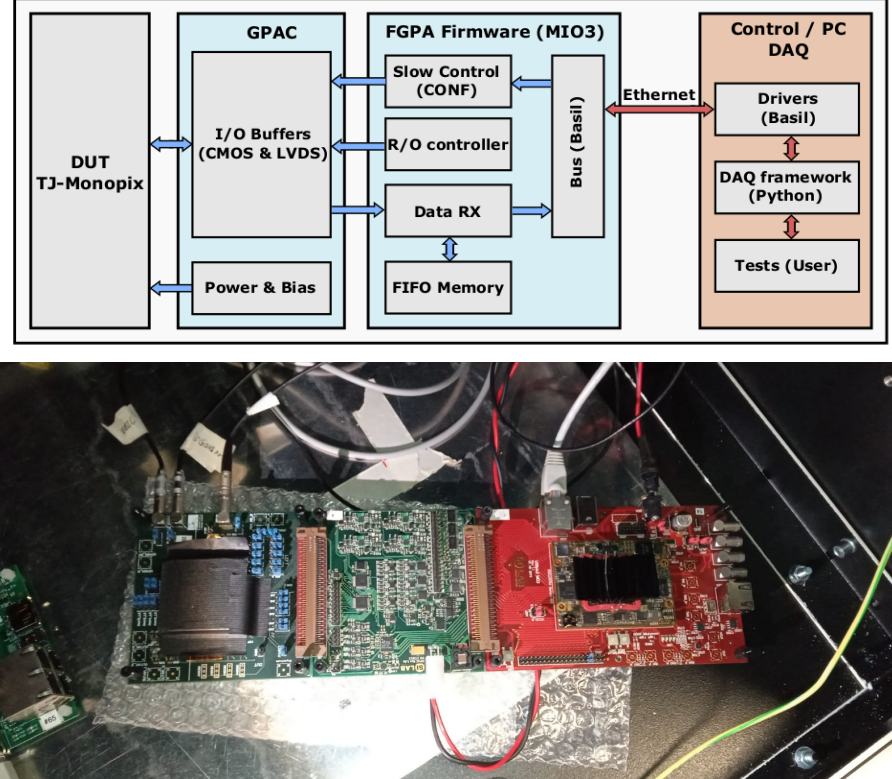
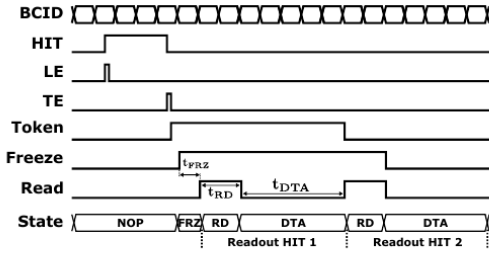


Figure 4.7: Main caption

551 After being read, the data packet is sent to the EoC periphery of the matrix, where a serializer
 552 transfers it off-chip to an FPGA (4.7). There a FIFO is used to temporarily stored the data, which
 553 is transmitted to a computer through an ethernet cable in a later time.

554 The access to the pixels' memory and the transmission of the data to the EoC, following
 555 a priority chain, is managed by control signals and is based on a Finite State Machine (FSM)
 556 composed by four state: no-operation (NOP), freeze (FRZ), read (RD) and data transfer (DTA).
 557 The readout sequence (??) starts with the TE of a pulse: the pixel immediately tries to grab the
 558 column-bus turning up a hit flag signal called *token*. The token is used to control the priority chain
 559 and propagates across the column indicating what pixel that must be read. To start the readout
 560 and avoid that the arrival of new hits disrupt the priority logic, a *freeze* signal is activated, and
 561 then a *read* signal controls the readout and the access to memory. During the freeze, the state of
 562 the token for all pixels on the matrix remains settled: this does not forbid new hits on other pixels
 563 from being recorded, but forbids pixels hit from turning on the token until the freeze is ended. The
 564 freeze stays on until the token covers the whole priority chain and gets the EoC: during that time
 565 new token cannot be turned on, and all hits arrived during a freeze will turn on their token at the
 566 end of the previous freeze. Since the start of the token is used to assign a timestamp to the hit,
 567 the token time has a direct impact on the time resolution measurement; this could be a problem

coping with high hits rate.



(b) Readout sequence timing diagram. In this example two hits are being processed.

Figure 4.8: Readout timing diagram: in this example two hits are being processed

The analog FE circuit and the pixel control logic are connected by an edge detector which is used to determine the LE and the TE of the hit pulse (fig. 4.9): when the TE is stored in the first latch the edge detector is disabled and, if the FREEZE signal is not set yet, the readout starts. At this point the HIT flag is set in a second latch and a token signal is produced and depending on the value of Token in the pixel can be read or must wait until the Token in is off. In figure an OR is used to manage the token propagation, but since a native OR logic port cannot be implemented with CMOS logic, a sum of a NOR and of an inverter is actually used; this construct significantly increases the propagation delay (the timing dispersion along a column of 0.1-0.2 ns) of the token and to speed up the circuit optimized solution are often implemented. When the pixel become the next to be read in the queue, and at the rising edge of the READ signal, the state of the pixel is stored in a D-latch and the pixel is allowed to use the data bus; the TE and the HIT flag latches are reset and a READINT signal that enable access of the RAM and ROM cells is produced.

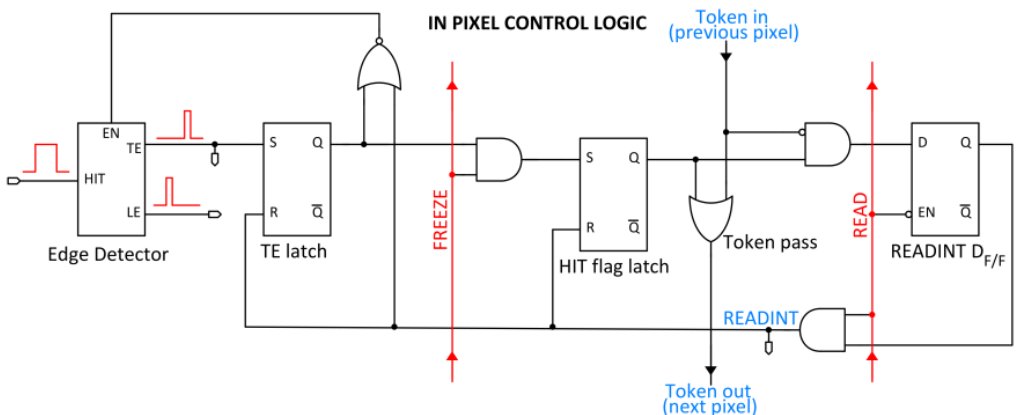


Figure 4.9

The final data must provide all the hits' information: the pixel address, the ToT and the timestamp. All those parts are assigned and appended at different time during the R/O chain:

- **Pixel address:** while the double column address (6-bit) is appended by the EoC circuit, the row address (8-bits for each flavor) and the physical column in the doublet (1-bit) are assigned by the in-pixel logic
- **ToT:** is obtained offline from the difference of 6-bits TE and 6-bits LE, stored by the edge detector in-pixel; since a 40 MHz BCID is distributed across the matrix, the ToT value is range 0-64 clock cycle which corresponds to 0-1.6 μ s
- **Timestamp:** The timestamp of the hit correspond to the time when the pixel set up the token; it is assigned by the FPGA, that uses the LE, TE and a 640 MHz clock to derive it. For all those hits which arrived while the matrix is frozen, the timestamp is no more correlated with the time of arrival of the particle

Parameter	Value [DAC]	Value [μs]
START_FREEZE	64	1.6
STOP_FREEZE	100	2.5
START_READ	66	1.65
STOP_READ	68	1.7

Table 4.4: Default configuration of the R/O parameters

594 When the bits are joined up together the complete hit data packet is 27-bit.

595 4.3.1 Dead time measurements

596 The hit loss is due to analog and digital pile up: the first one occurs when a new hit arrives during
 597 the pre-amplifier response, the second instead, which is the more relevant contribution, while the
 598 information of the previous hit has not yet been transferred to the periphery. As only one hit at
 599 a time can be stored on the pixel's RAM, until the data have completed the path to get out, the
 600 pixel is paralyzed and the dead time τ almost corresponds with the time needed to transmit the
 601 data-packets off-chip. Since the exportation of data from pixel to the EoC occurs via a 21-bits
 602 data bus, only one clock cycle is needed to transfer the data to the end of column and the dead time
 603 bottleneck is given by the bandwidth of the serializer at the EoC. In our setup it operates at 40
 604 MHz, thus to transmit a data packet (27-bit) at least 675 ns are needed. For what we have said so
 605 far, the R/O is completely sequential and therefore is expected a linear dependence of the reading
 606 time on the number of pixels to read:

$$\tau = 25 \text{ ns} \times (\alpha N + \beta) \quad (4.3)$$

607 where α and β are parameters dependent on the readout chain setting.

608 To measure and test the linearity of the reading time with the number of pixels firing, I have
 609 used the injection mode available on the chip. Indeed, the injection mode allows fixing not only
 610 the amplitude of the pulse, which corresponds to the charge in DAC units, but also the period and
 611 the width. I have injected a fix number of pulses (100) and looked for the rate when the efficiency
 612 decreases. Moreover to test that there is no dependence of the digital readout time from the charge
 613 of the pulse, I have tried to change the amplitude of the pulse injected, but the parameters found
 614 were consistent with the default configuration ones.

615 **Un esempio se leggo un singolo pixel: LA SLOPE CON CUI L'EFFICIENZA SCENDE È
 616 ABBSTANZA UNIFORME? perché satura a 50?**

617 While the single pixel reading time and the dead time do not depend on the position on the
 618 pixel matrix and are equal to 106 (46+60) clock counts within 1 clock count, on the other hand the
 619 τ depends on the pixel position on the matrix when more than one pixel are firing. In particular
 620 the priority chain goes from row 224 to row 0, and from col 0 to 112, that means the last pixels to
 621 be read is the one on the bottom right corner of the matrix.

622 In figure 4.11 is reported the reading time versus the number of pixels injected; the R/O
 623 parameters that control the reading time and their default values are reported on table ??.

624 The factor α , referring to eq. 4.3 is proportional to the difference (STOP_FREEZE - START_READ),
 625 while the offset β lies between 5 and 15 clock counts. Since through the injection a random hit rate
 626 on the matrix can't be simulated, as the coordinates of the pixels to inject must be specified, for
 627 convenience I used the pixels on the same column/row. No difference in the α and β coefficients
 628 has been observed between the two cases.

629 **A tutte le hit di una iniezione che arrivano contemporaneamente viene assegnato lo stesso
 630 timestamp; Risoluzione temporale??**

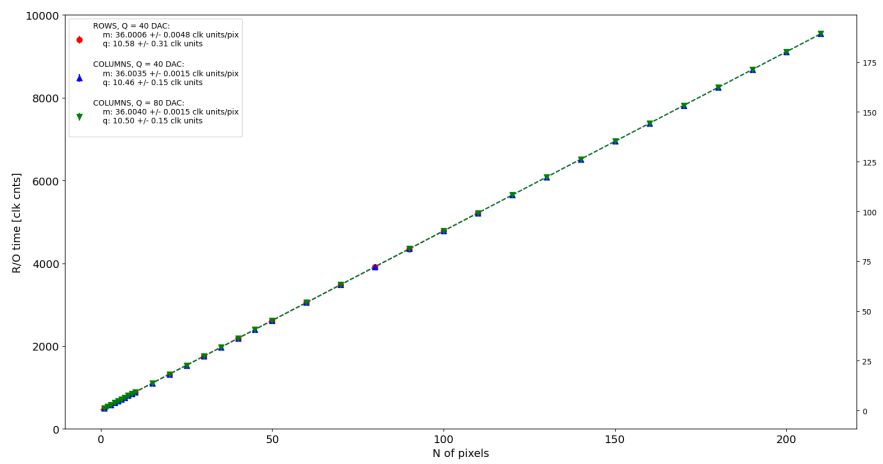


Figure 4.10

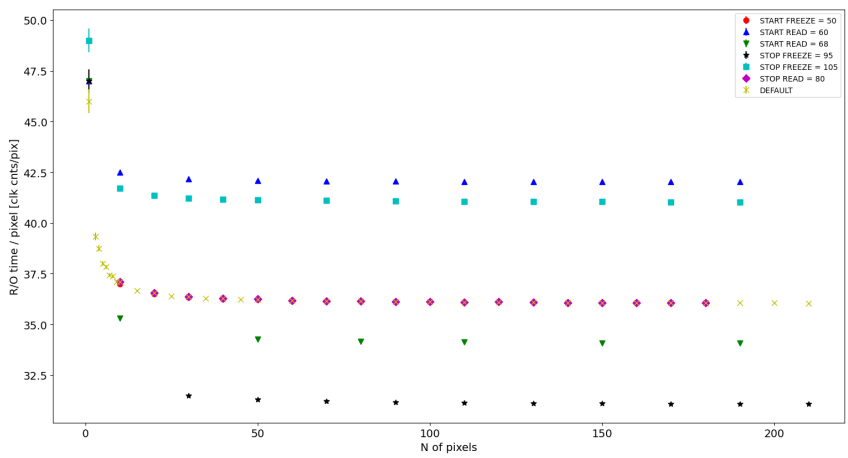


Figure 4.11

631 Chapter 5

632 Arcadia-MD1

633 [10] [11]

634 Breve introduzione analoga a Monopix1 in cui descrivo brevemente la "timeline" da SEED
635 Matisse a Md1 e Md2

636 5.1 The sensor

637 ARCADIA-MD1 is an LFoundry chip which implements the technology 110 nm CMOSS node
638 with six metal layer ???. The standard p-type substrate was replaced with an n-type floating zone
639 material, that is a tecnique to produce purified silicon crystal. (pag 299 K.W.).

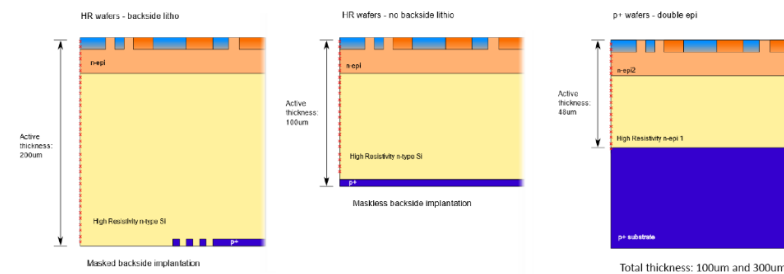


Figure 5.1

640
641 Wafer thinning and backside litography were necessary to introduce a junction at the bottom
642 surface, used to bias the substrate to full depletion while maintaining a low voltage at the front side.
643 C'è un deep pwell per - priority chainseparare l'elettronica dal sensore; per controllare il punchthought
644 è stato aggiunto un n doped epitaxial layer having a resistivity lower than the substrate.

645 RILEGGI SUL KOLANOSKY COS'È IL PUNCHTHROUGHT, FLOAT ZONE MATERIAL,
646 COME VENGONO FATTI I MAPS COME FAI LE GIUNZIONI

647 It is part of the cathegory of DMAPS Small electrode to enhance the signal to noise ratio.
648 It is operated in full depletion with fast charge collection by drift.

649 Prima SEED si occupa di studiare le prestazioni: oncept study with small-scale test struc-
650 ture (SEED), dopo arcadia: technology demonstration with large area sensors Small scale demo
651 SEED(sensor with embedded electronic developement) Quanto spazio dato all'elettronica sopra il
652 pwell e quanto al diodo. ..

653 5.2 Readout logic and data structure

654 5.2.1 Matrix division and data-packets

655 The matrix is divided into an internal physical and logical hierarchy: The 512 columns are divided
656 in 16 section: each section has different voltage-bias + serializzatori. Each section is devided in

657 cores () in modo che in ogni doppia colonna ci siano 1Pacchetto dei dati 6 cores. ricordati dei serializzaatori: sono 16 ma possono essere ridotti ad uno in modalità spazio

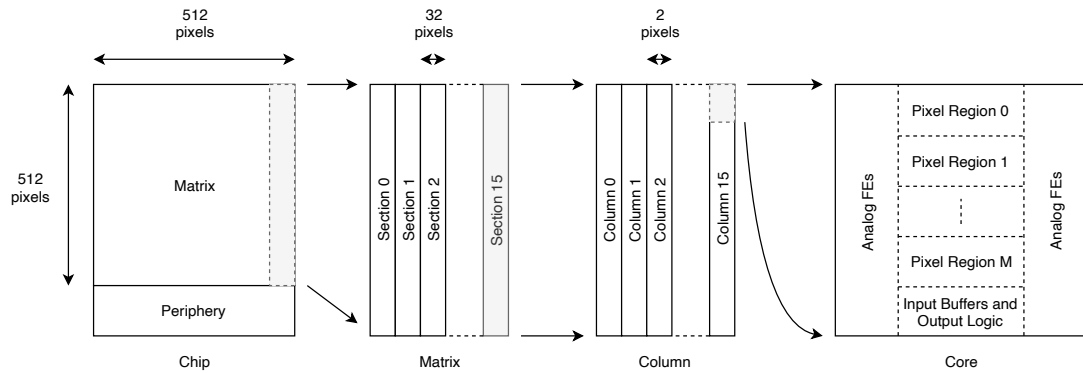


Figure 5.2

658

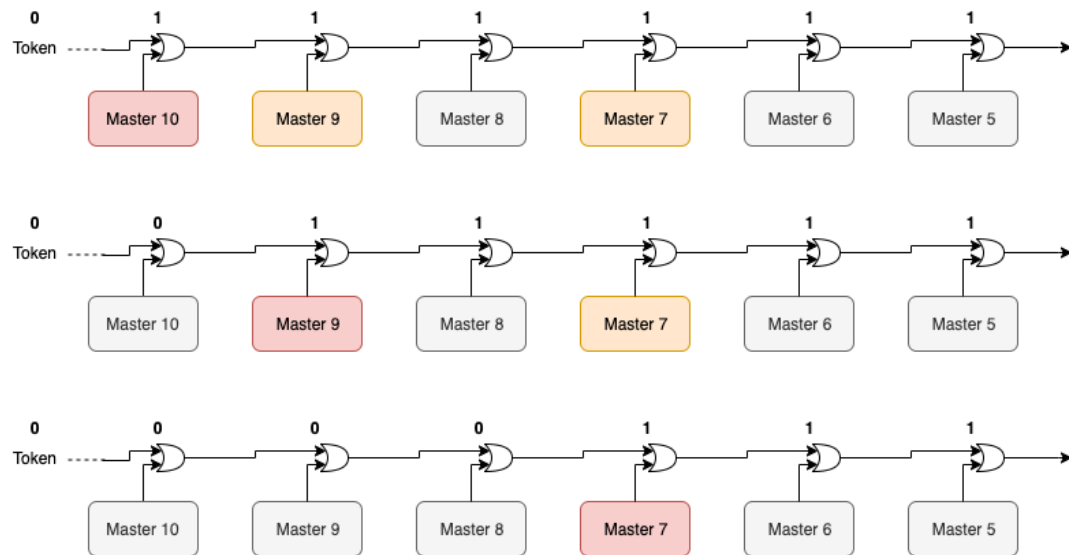


Figure 5.3

659 Questa divisione si rispecchia in come sono fatti i dati: scrivi da quanti bit un dato è fatto e le
660 varie coordinate che ci si trovano dentro; devi dire che c'è un pixel hot e spieghi dopo a cosa serve,
661 e devi accennare al timestamp

662 "A core is simply the smallest stepped and repeated instance of digital circuitry. A relatively
663 large core allows one to take full advantage of digital synthesis tools to implement complex func-
664 tionality in the pixel matrix, sharing resources among many pixels as needed.". pagina 28 della
665 review.

666

667 TABELLA: con la gerarchia del chip Matrix (512x512 pixels) Section (512x32 pixels) Column
668 (512x2) Core (32x2) Region (4x2)

669 Nel chip trovi diverse padframe: cosa c'è nelle padframe e End of section.

670 "DC-balance avoids low frequencies by guaranteeing at least one transition every n bits; for
671 example 8b10b encoding n =5"

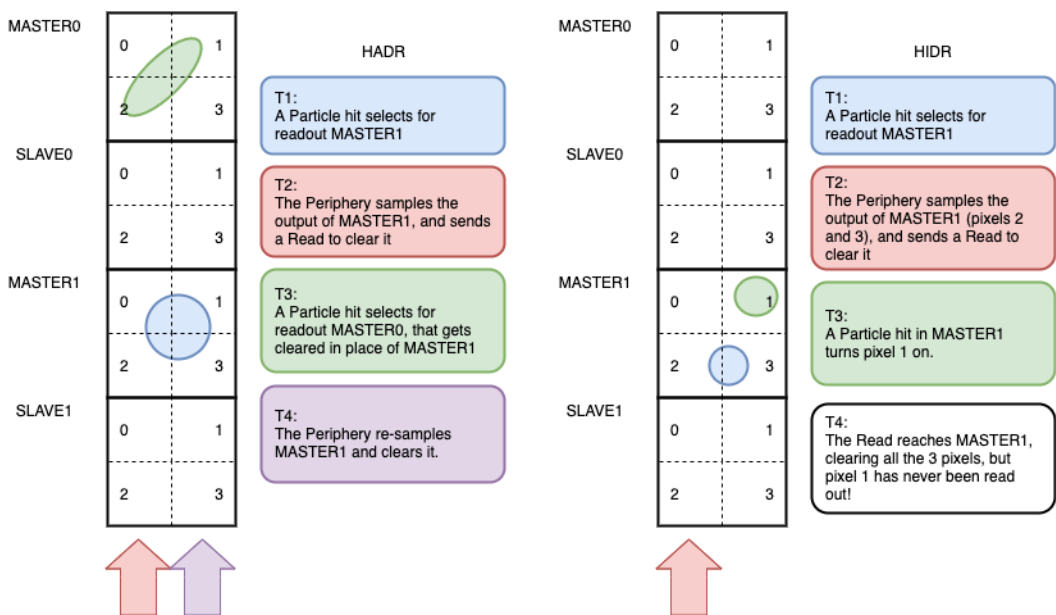


Figure 5.4

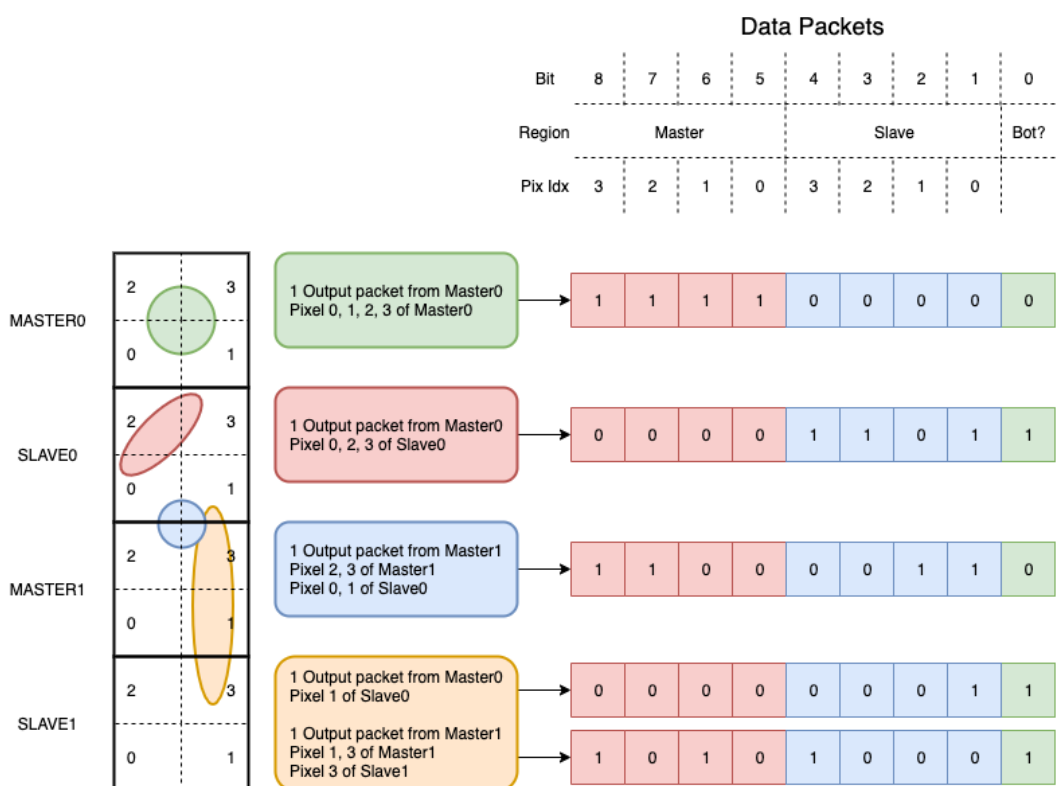


Figure 5.5

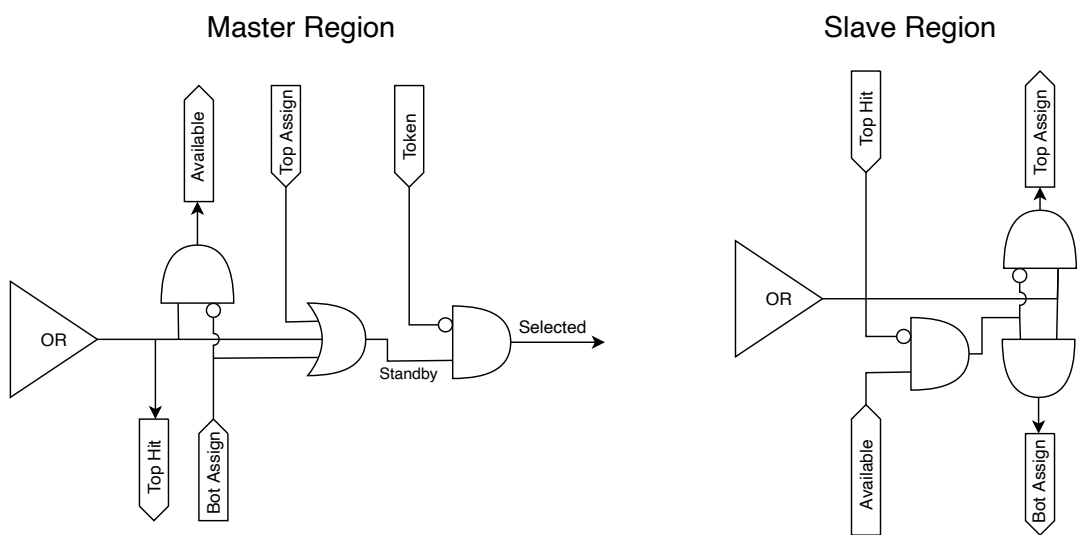


Figure 5.6

672 **Chapter 6**

673 **Threshold and noise
674 characterization**

675 **6.1 Threshold and noise: figure of merit for pixel detectors**

676 The signal to threshold ratio is the figure of merit for pixel detectors.

677 la soglia deve essere abb alta da tagliare il rumore ma abb bassa da non perdere efficienza.
678 Invece di prendere il rapporto segnale rumore prendi il rapporto segnale soglia. Perchè? la soglia
679 è collegato al rumore, nel senso che: supponiamo di volere un occupancy di 10-4 allora sceglierò la
680 soglia in base a questo. (plot su quaderno) Da questo conto trovo la minima soglia mettibile
681 In realtà quello che faccio è mettere una soglia un po' più grande perchè il rate di rumore dipende
682 da molti fattori quali la temperatura, l annealing ecc, e non voglio che cambiando leggermente uno
683 di questi parametri vedo alzarsi molto il rate di rumore. In realtà non è solo il rumore sensibile a
684 diversi fattori, ma anche la soglia: ad esempio la cosa classica è la variabilità della soglia da pixel
685 a pixel.

686 In questo modo rumore e soglia diventano parenti.

687 Review pag 26.

688 The noise requirement can be expressed as:

689 Questo implica tra le altre cose che voglio poter assegnare delle soglie diverse a diversi pixel:

690 Drawback è dare spazio per registri e quantaltro.

691 Questo lascia però ancora aperto il problema temporale delle variazioni del rumore: problema per
692 cui diventano necessarie le misure dei sensori dopo l'irraggiamento.

693 Per arcadia i registri (c'è un DAC) per la soglia (VCASN) si trovano in periferia. Non fare
694 trimming sulla soglia è uno dei problemi che si sono sempre incontrati: a casusa dei mismatch dei
695 transistor le soglie efficaci pixel per pixel cambiano tanto. La larghezza della s curve è il noise se se
696 assumi che il noise è gaussiano

697 Il trimming della soglia avviene con dei DAC: la dispersione della soglia dopo al tuning e dovuta
698 al dac è:

$$\sigma_{THR,tuned} = \frac{\sigma_{THR}}{2^{nbit}} \quad (6.1)$$

701 dove il numero di bit cambia varia tra 3-7 tipicamente. Monopix è 7 Arcadia 6

702 Each ROIC is different in this respect, but in general the minimum stable threshold was around
703 2500 electrons (e) in 1st generation ROICs, whereas it will be around 500 e for the 3rd generation.
704 This reduction has been deliberate: required by decreasing input signal values. Large pixels (2 104
705 um²), thick sensors (maggiore di 200 um), and moderate sensor radiation damage for 1st generation
706 detectors translated into expected signals of order 10 ke, while small pixels (0.25 104 um²), thinner
707 sensors (100 um), and heavier sensor radiation damage will lead to signals as low as 2 ke at the
708 HL-LHC

709 The ENC can be directly calculated by the Cumulative Distribution Function (CDF) (scurve)
710 obtained from the discriminator "hit" pulse response to multiple charge injections

⁷¹² **6.2 TJ-Monopix1 characterization**

⁷¹³ **6.3 ARCADIA-MD1 characterization**

714 **Chapter 7**

715 **Test beam measurements**

716 Epitaxial layer thickness: più grande è e più carica viene depositata da una MIP, però devi fare
717 attenzione alla forma della zona svuotata perchè può portare ad un aumento della charge sharing
718 tra pixel vicini. Se il diodo è molto piccolo rischi che l'efficienza di collection è diminuita perchè
719 l'intensità del campo elettrico è più bassa intorno al diodo, e hai più charge sharing.

720 Possibilità di integrare carica sul pixel: due elettroni consecutivi su un pixel ogni quanto ar-
721 rivano? Fai il conto del tempo medio

723 Vogliamo sfruttare l'analog pile up, per fare questo dobbiamo fare attenzione a non finire nel
724 digital pile up Devi avere che il tot dell'elettrone (cioè MIP) è maggiore del deltat medio; in questo
725 caso potresti riuscire ad integrare carica.

⁷²⁶ **Appendix A**

⁷²⁷ **Pixels detector: a brief overview**

⁷²⁸ **A.1 Radiation damages**

⁷²⁹ Radiation hardness is a fundamental requirement for pixels detector especially in HEP since they
⁷³⁰ are almost always installed near the interaction point where there is a high energy level of radiation.
⁷³¹ At LHC the ϕ_{eq} per year in the innermost pixel detector is $10^{14} n_{eq}/cm^2$; this number reduces by
⁷³² an order passing to the outer tracker layer [2] pag 341 Wermes. Here the high fluence of particles
⁷³³ can cause a damage both in the substrate of the detector and in the superficial electronics.

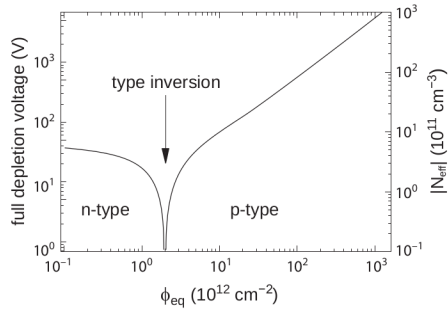
⁷³⁴ The first one has a principal non ionizing nature, due to a non ionizing energy loss (NIEL), but
⁷³⁵ it is related with the dislocation of the lattice caused by the collision with nuclei; by this fact the
⁷³⁶ NIEL hypothesis states that the substrate damage is normalized to the damage caused by 1 MeV
⁷³⁷ neutrons. Differently, surface damages are principally due to ionizing energy loss.

⁷³⁸ **DUE PAROLE IN PIÙ SUL SURFACE DAMAGE** A charge accumulation in oxide (S_iO_2) can
⁷³⁹ cause the generation of parasitic current with an obvious increase of the 1/f noise. Surface damages
⁷⁴⁰ are mostly less relevant than the previous one, since with the development of microelectronics and
⁷⁴¹ with the miniaturization of components (in electronic industry 6-7 nm transistors are already used,
⁷⁴² while for MAPS the dimensions of components is around 180 nm) the quantity of oxide in circuit
⁷⁴³ is reduced.

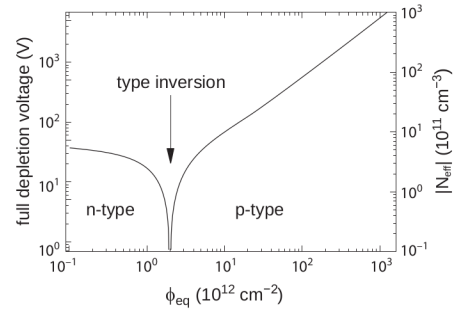
⁷⁴⁴ Let's spend instead two more other words on the more-relevant substrate damages: the general
⁷⁴⁵ result of high radiation level is the creation of new energy levels within the silicon band gap and
⁷⁴⁶ depending on their energy-location their effect can be different, as described in the Shockely-Read-
⁷⁴⁷ Hall (SRH) statistical model. The three main consequence of radiation damages are the changing
⁷⁴⁸ of the effect doping concentration, the leakage current and the increasing of trapping probability.

⁷⁴⁹ **Changing of the effective doping concentration:** is associated with the creation/removal
⁷⁵⁰ of donors and acceptors center which trap respectively electrons/holes from the conduction band
⁷⁵¹ and cause a change in effective space charge density. Even an inversion (p-type becomes n-type¹)
⁷⁵² can happen: indeed it is quite common at not too high fluences ($\phi_{eq} 10^{12-13} n_{eq} cm^{-2}$). A changing
⁷⁵³ in the doping concentration requires an adjustment of the biasing of the sensor during its lifetime
⁷⁵⁴ (eq.2.1) and sometimes can be difficult keeping to fully deplete the bulk.

¹L'INVERSIONE OPPOSTA NON CE L'HA PERCHÈ?



(a) 1a



(b) 1b

755 **Leakage current:** is associated with the generation-recombination centers. It has a strong
756 dependence with the temperature ($I_{leak} \propto T^2$), whose solution is therefore to operate at lower
757 temperature.

758 **Increase of trapping probability:** since the trapping probability is constant in the depleted
759 region, the collected charge decreases exponentially with the drift path. The exponential coefficient,
760 that is the mean trapping path, decreases after irradiation and typical values are 125-250 μm and
761 must be compared with the thickness of the depleted region which () corresponds to the mean drift
762 path.

763 Different choices for substrate resistivity, for junctions type and for detector design are typically
764 made to fight radiation issues. Some material with high oxygen concentration (as crystal produced
765 using Czochralki (Cz) or float-zone (Fz) process (**CONTROLLA LA DIFFERENZA TRA I DUE**))
766 for example, show a compensation effect for radiation damage; another example is the usage of
767 n+ -in-p/n sensors (even if p+ -in-n sensors are easier and cheaper to obtain) to get advantage
768 of inversion/to have not the inversion (since they are already p-type). After inversion the n+p
769 boundary, coming from n+ in-n, but to keep using the sensor the depletion zone still must be
770 placed near the diode.

⁷⁷¹ Appendix B

⁷⁷² FLASH radiotherapy

⁷⁷³ La radioterapia si usa nel 60 per cento dei pazienti, sia come cura che come trattamento palliativo.
⁷⁷⁴ Si associa spesso ad altre cure e si può fare prima/durante/dopo un intervento.

⁷⁷⁵
⁷⁷⁶ Si può fare in modi diversi: da dentro (brachytherapy) oppure da fuori (quella standard). Un
⁷⁷⁷ requisito importante è la delinazione del target (non vuoi rischiare di beccare i tessuti sani), per
⁷⁷⁸ cui prima tipicamente si fanno esami di imaginig del tumore. Tipicamente anche gli acceleratori
⁷⁷⁹ stessi per la terapia sono provvisti di radiografia.

⁷⁸⁰ Un problema dei fotoni ad esempio è che il loro rilascio di dose è lineare, per cui danneggia
⁷⁸¹ anche i tessuti sani. Il problema dei protoni invece è che hanno un picco troppo stretto per cui non
⁷⁸² puoi coprire grosse zone e soprattutto se sbagli rischi davvero di danneggiare molto i tessuti sani.

⁷⁸³

⁷⁸⁴ B.1 Cell survival curves

⁷⁸⁵ Curva di efficacia del trattamento in funzione della dose:

$$\frac{S(D)}{S(0)} = e^{-F(D)} \quad (\text{B.1})$$

⁷⁸⁶ dove $F(D)$

$$F(D) = \alpha D + \beta D^2 \quad (\text{B.2})$$

⁷⁸⁷ dove α e β rappresentano due tipi di danno diversi: coefficients, experimentally determined, characterizing the radiation response of cells. In particular, alpha represents the rate of cell killing by single ionizing events, while beta indicates the maximal rate of cell killing by double hits observed when the repair mechanisms do not activate during the radiation exposure. Si ottiene una curva di sopravvivenza dove si vede la possibilità delle cellule di autoripararsi. A basse dosi infatti le cellule possono ripararsi.

⁷⁸⁸

⁷⁹⁴ Per introdurre l'effetto FLASH introduco prima la therapeutic window.

⁷⁹⁵

⁷⁹⁶ TCP è la tumor control Probability che indica la probabilità delle cellule del tumore di essere uccise dopo una certa dose (con in riferimento a dose in acqua)

⁷⁹⁷ Se una media di $\mu(D)$ di cellule di tumore are killed con una dose D, la probabilità che n cellule sopravvivono è data da $P(n|\mu)$ poisson:

$$P(n|\mu) = \frac{\mu(D)^n e^{-\mu(D)}}{n!} \quad (\text{B.3})$$

$$TCP(D) = P(n=0|\mu(D)) = e^{-\mu(D)} \quad (\text{B.4})$$

⁸⁰⁰ D'altra parte hai una probabilità di fare danno su normal tissue NTCP Normal Tissue Complication Probability, che rappresenta il problema principale e che limita la massima radiazione erogabile
⁸⁰¹ Una scelta bilanciata si applica guardando a questi due fattori; si usa il therapeutic index definito
⁸⁰² come TCP/NTCP.

804 La cosa ottimale è ampliare la finestra del therapeutic ratio.

805 CONV-RT 0.01-5 Gy/min. A typical RT regime today consists of daily fractions of 1.5 to 3
806 Gy given over several weeks.

808 Nell Intra operative radiation therapy (IORT), where they reach values respectively about 20 and
809 100 times greater than those of conventional radiation therapy.

810 FLASH vuole ultrahigh mean dose-rate (maggione di 40 Gy/s) in modo da ridurere anche il
811 trattamento a meno di un secondo.

812

813 **B.2 FLASH effect**

814 Ci sono due effetti che affect the flsh effect and la sua applicabilità: Dose rate effect e oxygen

815

816 Cellule che esibiscono hypoxia (cioè cellule che non hanno ossigeno sono radioresistenti); al
817 contrario normoxia e physoxia non lo sono. la presenza di ossigeno rende la curva steeper indicando
818 che lo stesso danno si raggiunge a livelli di dose più bassi rispetto al caso senza ossigeno.

819 FIGURA con una curva a confronto con e senza ossigeno.

820 Typically, the OER is in the order of 2.5–3.5 for most cellular systems

821 Quindi si vogliono sfruttare questi effetti per diminuire la tossicità sui tessuti sani

822

823 Bibliography

- 824 [1] W. Snoeys et al. “A process modification for CMOS monolithic active pixel sensors for
825 enhanced depletion, timing performance and radiation tolerance”. In: (2017). DOI: <https://doi.org/10.1016/j.nima.2017.07.046>.
- 826 [2] H. Kolanoski and N. Wermes. *Particle Detectors: Fundamentals and Applications*. OXFORD
827 University Press, 2020. ISBN: 9780198520115.
- 828 [3] E. Mandelli. “Digital Column Readout Architecture for the ATLAS Pixel 0.25 um Front End
829 IC”. In: (2002).
- 830 [4] M. Garcia-Sciveres and N. Wermes. “A review of advances in pixel detectors for experiments
831 with high rate and radiation”. In: (2018). DOI: <https://doi.org/10.1088/1361-6633/aab064>.
- 832 [5] M. Dyndal et al. “Mini-MALTA: Radiation hard pixel designs for small-electrode monolithic
833 CMOS sensors for the High Luminosity LHC”. In: (2019). DOI: <https://doi.org/10.1088/1748-0221/15/02/p02005>.
- 834 [6] M. Barbero. “Radiation hard DMAPS pixel sensors in 150 nm CMOS technology for opera-
835 tion at LHC”. In: (2020). DOI: <https://doi.org/10.1088/1748-0221/15/05/p05013>.
- 836 [7] K. Moustakas et al. “CMOS Monolithic Pixel Sensors based on the Column-Drain Architec-
837 ture for the HL-LHC Upgrade”. In: (2018). DOI: <https://doi.org/10.1016/j.nima.2018.09.100>.
- 838 [8] I. Caicedo et al. “The Monopix chips: depleted monolithic active pixel sensors with a column-
839 drain read-out architecture for the ATLAS Inner Tracker upgrade”. In: (2019). DOI: <https://doi.org/10.1088/1748-0221/14/06/C06006>.
- 840 [9] D. Kim et al. “Front end optimization for the monolithic active pixel sensor of the ALICE
841 Inner Tracking System upgrade”. In: *JINST* (2016). DOI: doi:10.1088/1748-0221/11/02/
842 C02042.
- 843 [10] L. Pancheri et al. “A 110 nm CMOS process for fully-depleted pixel sensors”. In: (2019). DOI:
844 <https://doi.org/10.1088/1748-0221/14/06/c06016>.
- 845 [11] L. Pancheri et al. “Fully Depleted MAPS in 110-nm CMOS Process With 100–300-um Active
846 Substrate”. In: (2020). DOI: 10.1109/TED.2020.2985639.